NTNU

Norwegian University of
Science and Technology

Full-waveform inversion studies

Espen Thomassen

Master of Science in Electronics
Submission date: June 2008
Supervisor: Hefeng Dong, IET
Co-supervisor: Celine Ravaut, SINTEF Petroleum Research

Norwegian University of Science and Technology
Department of Electronics and Telecommunications

Problem Description

Seismic depth imaging is now the preferred seismic imaging tool for today's most challenging exploration projects. Seismic depth imaging problem usually requires the definition of a smooth background velocity model before determining the shortwavelength component of the structure by pre-stack depth migration. It is well established that success of pre-stack depth migration in complex geological media strongly depends from the definition of the background velocity model.

In SINTEF, our in-house stereotomographic method is used to define the background velocity model before running our 2D pre-stack depth migration tool. Recently, we investigated the idea of including a full-waveform inversion method to refine the background velocity model derived from stereotomography before applying the depth
migration tool in order to improve imaging in complex geological areas.

The objective of this master project will consist in applying our full waveform inversion method in a complex sub-salt geological setting. It is, indeed, well known
that classical imaging techniques usually fail to image beneath salt screen as strong velocity contrasts between the salt and the surrounding sediments usually complicate
the seismic wave propagation and lead to significant problems. A recent application of full-waveform inversion to sub-salt dataset showed that this method is a good
alternative to improve imaging in these contexts. In this project, we would like to estimate the capabilities and the limits of our in-house full-waveform inversion tool to
improve velocity model building when applied to synthetic sub-salt dataset.

The student will first have to evaluate the capability of the technique itself in this context. He/She will have to estimate if stereotomography or first-arrival traveltime
tomography enables to derive velocity models precise enough to initiate fullwaveform inversion. As full-waveform inversion is known to be sensitive to initial
velocity model and initial inverted frequency, he/she will also have to define the optimal parameters to ensure the success of the method in this complex sub-salt case
and find ways to evaluate quantitatively the quality of the results obtained in these conditions.

The student will have to familiarize with our in-house full seismic depth imaging flow. He/She will familiarize with seismic inversion problems and get experience on
tomographic methods. He/She will also get experience on application to dataset in complex geological area. He/She will also have the opportunity to work on a "hot topic" of seismic imaging.

Assignment given: 15. January 2008
Supervisor: Hefeng Dong, IET

Acknowledgements

This master thesis is the final piece of obtaining my Master of Science degree at the Norwegian University of Science and Technology (NTNU), Department of Electronics and Telecommunications. The assignment was proposed by SINTEF Petroleum Research in Trondheim, and I would like to thank them for giving me the opportunity to perform this work.

I would specially like to thank my supervisor at SINTEF, Dr. Céline Ravaut, for all her patience, help and guidance. I would also like to thank my supervisor at NTNU, Prof. Hefeng Dong for the help she has given me.

Espen Thomassen
Trondheim, June 7, 2008

Summary

In this master thesis, full-waveform inversion (FWI) was applied to a synthetic, and very complex, geological structure containing a salt body. The main objective was to evaluate the capabilities of FWI to estimate velocities in this context, and more specially below the salt.

Seismic depth imaging is now the preferred seismic imaging tool for today's most challenging exploration projects. Seismic depth imaging problem usually requires the definition of a smooth background velocity model before determining the short wavelength component of the structure by pre-stack depth migration. It is well established that success of pre-stack depth migration in complex geological media strongly depends from the definition of the background velocity model. Standard tools for building velocity models generally fail to reconstruct the correct sub-salt velocities. Sub-salt imaging is a very challenging problem and a lot of resources are spent trying to solve this problem, since salt bodies in the sub-surface are known to be very good hydrocarbon traps.

In this master thesis, the work have been performed on a modified version of the 2004 BP velocity benchmark model. This model represents a very interesting salt context, where conventional imaging methods can not provide any good results. After describing the seismic inversion problem, and the FWI theory and code used in this work, the application to the 2004 BP benchmark model is described.

FWI was first applied to the synthetic data using a starting model derived by smoothing the true velocity model. This is an easy way to ensure an adequate starting model, as the method is very dependent on a good starting model. In the inversion process 17 frequency components were used, ranging between 1 and 15 Hz. This resulted in a velocity model that accurately recovered both the salt body and the sub-salt velocities. The average deviation between the true and estimated sub-salt velocities was found to be approximately 6 %.

A more realistic starting model was then derived using first-arrival traveltime tomography, a well known method for obtaining velocity models. FWI was

applied to this starting model, and the result was also positive when using this starting model. The salt body was well delineated, whereas the sub-salt velocities were generally more inaccurate than for the previous application. The sub-salt velocity difference was increased to roughly 10 %. However, if more effort had been spent on reconstructing a more accurate starting model, the results might have improved.

When fewer frequency components are used in the inversion, the result declined. A test using only 6 frequency components showed that the final reconstructed model suffered from a lack of recovered wavenumbers, especially at the deeper and more complex parts of the model. In such a complex medium as the 2004 BP benchmark model, it is hence necessary to introduce wavenumbers by including a sufficient number of frequency components in the inversion process.

Other tests that were conducted showed that, in this particular case, the non-linearity of the inversion problem increased with higher frequencies, and was reduced by larger offset ranges included in the seismic data. The inversion is hence sensitive to the starting frequency as well as the starting model.

The results in this master thesis demonstrate that FWI has a great potential in reconstructing sub-salt velocities in salt media. For the future, both applying the method to real data from a salt basin area, and develop a migration tool and test the effect of FWI on a migrated image, are interesting challenges.

Contents

List of Figures

Chapter 1

Introduction

Information about the sub-surface can be derived from recordings of seismic waves travelling in the earth. In seismic exploration, such seismic waves are generated by artificial sources and recorded by hydrophones/geophones at the surface, after propagating through the medium of interest. The seismic recordings are called seismograms or seismic traces. Since the waves are affected by the physical properties of the sub-surface, they are carrying information about the medium that can be retrieved by an inversion process. Industrial seismic explorations are commonly conducted when looking for hydrocarbons.

Today, seismic depth imaging is the preferred tool for seismic imaging of complex geological structures. This method consists in the definition of a smooth background velocity model before determining the short wavelength components of the structure by pre-stack depth migration. The pre-stack depth migration method aims to locate the seismic reflected events to their correct location in depth. To be successful, this technique requires an accurate knowledge of the velocities of the ground. The estimation of a velocity model is a difficult process, especially when velocities vary rapidly in both lateral and vertical directions. Full-waveform inversion (FWI) is a tool for building such velocity models. If the velocity model includes both low *and* intermediate wavenumbers, the pre-stack depth migration will be improved (Sirgue, 2003). FWI have the potential to recover a continuous range of wavenumbers of a complex structure.

Classical seismic imaging techniques usually fail when applied to a complex geological structure specially including a salt body. Indeed, the velocity contrast between the salt and the surrounding sediments usually complicates the propagation of the seismic wave, thus making the imaging of the salt body and specially the sub-salt structure quite difficult. Retrieving sub-salt information is an issue of interest for many parts, as salt bodies can

hide reservoirs of hydrocarbons. Full-waveform inversion might be a good alternative to recover sub-salt velocities and hence to improve the imaging process in these contexts. The main objective of this master thesis was to apply SINTEF Petroleum Research's FWI code to investigate the capabilities and the limits of this method to improve sub-salt imaging from a synthetic data-set. To do so, answers to the following were tried to be found.

- What can be recovered when FWI is applied on a complex structure containing a salt body. Can velocities be well recovered below the salt?
- What is important for the full-waveform inversion to be able to recover velocities below the salt. What are the parameters that ensure the success of the method, and what are the limitations of the method?
- What are the differences between FWI and other methods, such as first-arrival traveltime tomography?

In addition, this master thesis should present the theory and give an introduction about full-waveform inversion in general.

Presentation of the synthetic model

The model used for testing the capabilities of full-waveform inversion in this master thesis, is a sub-section of the 2004 BP velocity benchmark model (Billette and Brandsberg-Dahl, 2005) as seen on figure 1.1. This model was specially created by BP for velocity analysis and testing the velocity model building tools. The first results using this model were, according to the authors, presented at a workshop during the 2004 EAGE conference (Billette and Brandsberg-Dahl, 2005). The model can be divided in three distinctive parts, each presenting known seismic imaging challenges. The left part of the model, which is the sub-section used in this master thesis, contains a large, complex, horizontal salt body and some sub-salt low velocity anomalies. This makes the medium very complex and the velocities in and below the salt were proven to be very difficult to estimate (Billette and Brandsberg-Dahl, 2005).

The original BP model (figure 1.1) is 67 km long by 12 km deep. The velocity parameters are built on a 12.5 m $\times$ 6.25 m grid, i.e. 5395 $\times$ 1911 grid points. The test medium, shown on figure 1.2, is however defined by 1201 $\times$ 401 grid points, re-sampled on a 15 $\times$ 15 m regular squared grid. The model of the thesis is hence decreased to 18 km in length by 6 km in depth. This modified model will be referred to as "the true model". The modifications of the original BP model were done in order to have a reasonable sized model to handle, and to focus in a complex part of the model. FWI uses a quite large amount of resources, so the number of grid points had to be reduced. In

addition, the left part of the BP benchmark model alone was a very suitable model for testing the sub-salt recovery capabilities of the FWI.

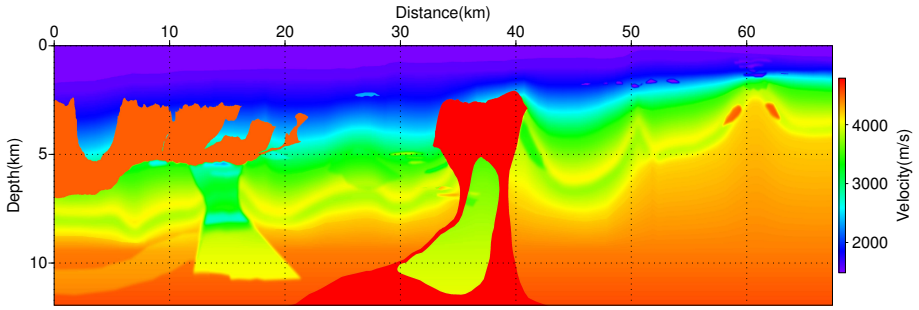

Figure 1.1: The original 2004 BP velocity benchmark model

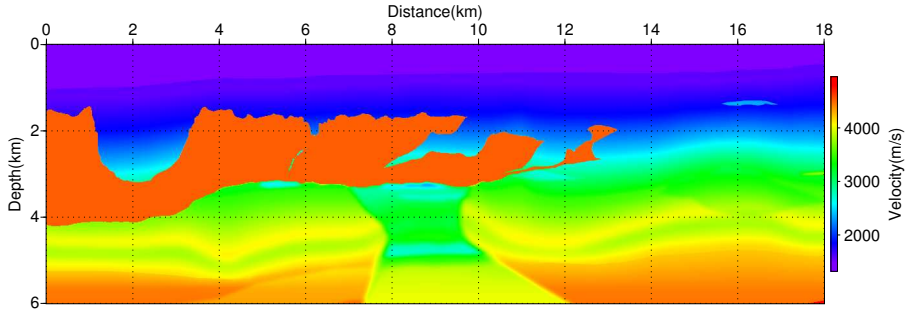

Figure 1.2: The modified velocity model used in this master thesis. This model is 18 km long by 6 km depth. It is defined by 1201 $\times$ 401 grid points spaced 15 m apart. Vertical and horizontal axes are in km. Velocity scales are in m/s, and range between 1480 and 4790 m/s

Contents of the master thesis

The first part of this master thesis is a general introduction to the inverse problem. The seismic inverse problem is presented, and why this problem is of any interest. Some techniques on how to solve it are also outlined. This is all included in chapter 2.

In chapter 3, first-arrival traveltime tomography is presented. This is a well known method for estimating velocity models. The SINTEF code for this method is described shortly, together with some background theory. The

method is applied to the sub-section of the 2004 BP benchmark model. First-arrival traveltime tomography can be suitable for obtaining starting models for full-waveform inversion, and the recovered velocity model in this chapter is used in that purpose in chapter 5.

The technique and theory of full-waveform inversion are explained in chapter 4. This chapter first gives an introduction of FWI, before some of the key elements of the code are presented.

In chapter 5, full-waveform inversion is applied to the very complex geological structure containing a salt body, i.e. the sub-part of the 2004 BP benchmark model. First a smoothed version of the true model is used as a starting model for the FWI, then the first-arrival traveltime model from chapter 3. Both inversion results are analysed and discussed. The chapter also investigates the influence of important inversion components such as the quality of the starting model, the number of inversion frequencies, and the starting frequency.

Conclusions and future work are covered in chapter 6.

Chapter 2

General inversion theory

Estimating the subsurface velocities from a seismic data set, as this thesis set out to do, is a so-called *inverse problem*. This chapter covers some of the basic ideas and theories necessary to solve such a problem.

2.1 Introduction

The aim of the seismic inverse problem is to estimate the earth's subsurface characteristic parameters from a seismic recording. The recorded wavefield data are known, while the physical properties of the medium which the wavefield have propagated through are the unknowns. Such a wavefield will be a function of the medium properties. Forward modelling is the opposite of an inverse problem. The physical properties of the medium are known, hence it is possible to compute the wavefield at any given time and location. The relationship between forward modelling and the inverse problem is shown on figure 2.1.

The relationship between data and model can either be linear or non-linear, and then described by the following equations

$$\vec{d} = G\vec{m} \quad \text{where } G \text{ is the linear operator} \tag{2.1}$$

$$\vec{d} = g(\vec{m}) \quad \text{where } g \text{ is the non-linear operator} \tag{2.2}$$

In these equations $\vec{d}$ is the wavefield, $\vec{m}$ is a model of the medium, and g, or G, is the known relationship between them.

Equations (2.1) and (2.2) represent forward modelling (computing data from a known model), while equation (2.3) below, represents the inverse problem

if g is invertible.

$$\vec{m} \approx g^{-1}(\vec{d}) \tag{2.3}$$

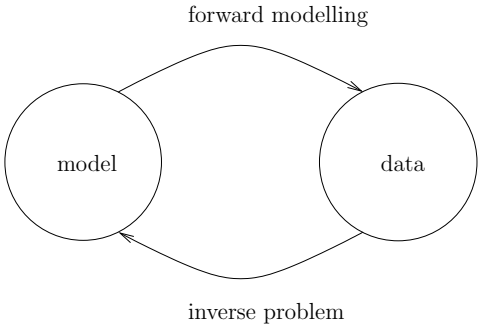

Figure 2.1: Simple sketch showing the relationship between forward modelling and inverse problem (from (Chabert, 2007))

Non-linear relations between model and data are a great challenge when solving the inverse problem. Looking at the plots in figure 2.2, the solution $f(x)$ can be found intrinsic by forward modelling if the x and the relationship f is known. For the inverse problem, the value of $f(x)$ and relationship f is known. In figure 2.2(a), which represents the linear relationship, the correct values of x_1 and x_2 can be derived from $f(x_1)$ and $f(x_2)$ respectively. On the other hand, when f is non-linear, as in figure 2.2(b), it is impossible to know if the value $f(x_1)$ originates from x_1 or x_3.

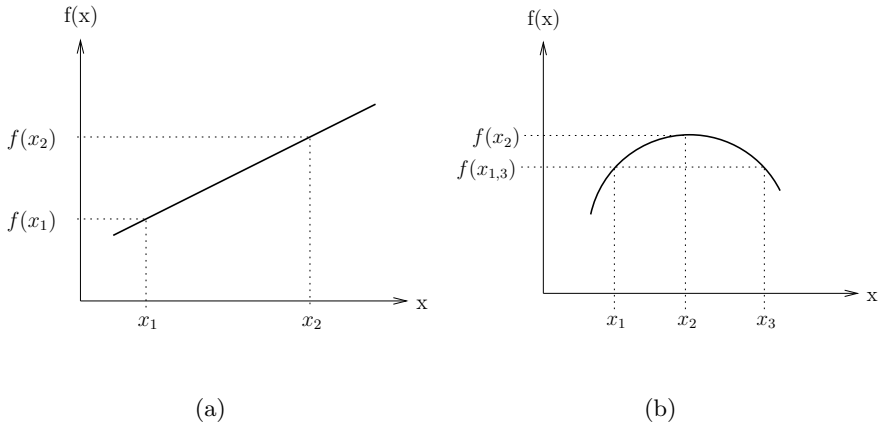

Figure 2.2: **(a)** Simple linear function. **(b)** Simple non-linear function

Geophysical problems are almost always non-linear (Chabert, 2007). The solution of the inversion is therefore not necessarily the true solution, but

a solution that explains the data. There can also be other solutions for a model that explains the data, so the solution is said to be non unique.

If the relationship, g, is only weakly non-linear, the problem can be linearised and a solution of the problem can be found by local methods (section 2.3.2). If the non-linearity is too strong, global methods have to be used in the search for the correct estimation of the model parameters (section 2.3.1).

2.2 The forward modelling

Forward modelling consists in computing the wavefield at a given time and a given position. This is done by solving the wave equation. Depending on the characteristics of the medium, the presence of a source, etc., the formulation of this equation might differ. For example, equation (2.4) is the acoustic, linear, lossless, homogeneous (no source) wave equation (Kinsler et al., 2000). p is the pressure, c is the sound velocity, and ∇^2 denotes the Laplacian operator.

$$\nabla^2 p = \frac{1}{c^2}\frac{\partial^2 p}{\partial t^2} \tag{2.4}$$

The methods for solving the wave equation can be generalized as one of the following:

1. Analytical solutions
2. Integral solutions
3. Ray theory
4. Numerical methods

The wave equation can only be solved analytically if the medium is homogeneous. An analytic solution is the only method that gives an exact solution not based on approximations and simplifications.

Integral solutions to the wave equation can be carried out in the (k, ω) space (wavenumber, frequency), by summation of elementary analytical solutions. The integral methods are extremely precise, but they are limited to stratified or simple media. Integral methods are for example the reflectivity method (Fuchs and Müller, 1971) and the discrete wavenumber method (Bouchon and Aki, 1977)

In ray theory, the wave equation is solved by asymptotic, high-frequency approximation (Červený et al., 1977). Ray tracing theory looks at wave propagation as rays following the normal component of the wavefront. When

the velocity of the medium is constant, the ray path will be straight, but if the velocity is increasing or decreasing, the ray paths will curve. The rays will be reflected and/or transmitted at interfaces in a layered medium. Since the ray theory is a high frequency approximation it requires the wavelengths to be smaller than the velocity variations in the medium (Hovem, 2007).

Numerical methods can be, e.g. finite difference, finite element, finite volume and spectral element methods. The numerical methods seek the solution of differential equations by making approximations and simplifications for easy computing. Generally, these methods divide the spacing into a mesh, where calculations of node values contribute to the complete wavefield. This gives many, but simple, calculations. Numerical methods are well suited to find solution to the wave equation for complex and inhomogeneous media, but the calculations can be time consuming, especially in 3-D.

2.3 Solving the inverse problem

The seismic inversion problem consist of finding a set of model parameters ($\vec{m}$) that predicts the observed seismic data ($\vec{d}_{\text{obs}}$) (Pratt et al., 1998). A forward modelling routine computes a set of data ($\vec{d}_{\text{cal}}$) based on a current estimation of the model parameters. The residual between observed and computed data ($\vec{\delta d} = \vec{d}_{\text{obs}} - \vec{d}_{\text{cal}}$) should be as small as possible, and the model parameters can be updated to reduce this misfit. The model can be updated as in an optimization scheme. The process described above, can be illustrated as in figure 2.3.

The residuals that the optimization process will try to minimise can often be described by the ℓ^2-norm of the error between measured and calculated data (equation (2.5)).

$$\vec{E}(\vec{m}) = \frac{1}{2}\left\|\vec{d}_{\text{obs}} - \vec{d}_{\text{cal}}\right\|^2 = \frac{1}{2}\left\|\vec{\delta d}\right\|^2 = \frac{1}{2}\vec{\delta d}^{\,t}\,\vec{\delta d}^{\,*} \tag{2.5}$$

In equation (2.5), $\vec{\delta d}^{\,t}$ is the transposed matrix, and $\vec{\delta d}^{\,*}$ is the complex conjugation of the data residuals. The function $\vec{E}(\vec{m})$ will in this paper be referred to as "the cost function", even though "the object function", "the misfit function" and other names are found throughout the literature.

The model space consists of all possible models. The number of possible models is given by the possible distinct values of a parameter k, raised to the power of numbers of parameters, p, i.e. the model space is made of k^p models. When the earth is the medium, it can have an infinite number of parameter values, and therefore an infinite number of models in the model space. Even after the parameters have been discretised, the model space can

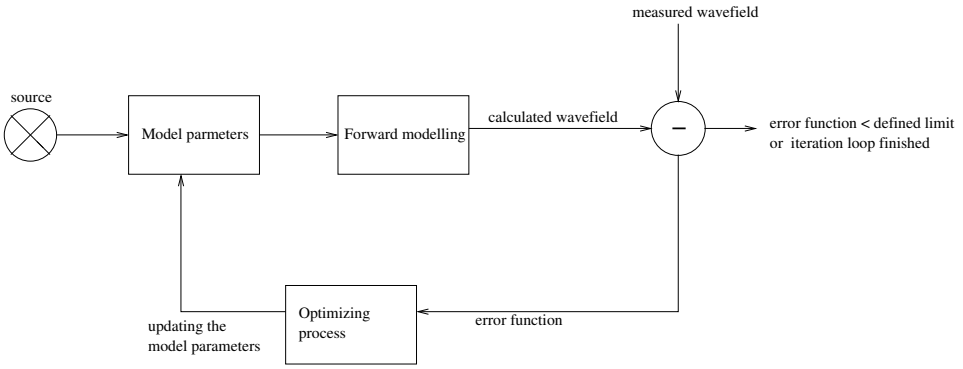

Figure 2.3: A schematic overview of the inverse problem solved as an optimizing process. A calculated wavefield can be computed by forward modelling in the current model estimation. This wavefield is compared to the observed wavefield. If the misfit is small enough the model is considered a good estimation of the true parameters. If not, the error function will be the input in an optimizing process updating the current model so that the misfit is reduced

be enormous. An exhaustive search for the best model is almost impossible regarding time consumption. More clever methods for finding a model describing the medium are hence necessary. There are two main categories of methods dealing with solving the inverse problem:

1. Global optimization methods
2. Linearising the problem and solving it directly

2.3.1 Global methods

If the problem is highly non-linear, global methods can be used for finding a model that explains the data. The Monte Carlo method is a well known global optimization method. At its simplest form, it chooses a pool of models from the total model space, runs forward modelling, and see what model has the lowest cost function. Two other global methods that have been shown more effective are the genetic algorithm and simulated annealing.

In the genetic algorithm method, a relatively small selection of models is chosen from the model space. The best models of this selection (parents) will form new models (children) by cross-over and mutation of the bit-strings describing the model parameters. The children will then replace the weakest models in the selection. By such iterative steps, the selection of models will gather towards a minimum of the cost function (Gerstoft, 1993).

In simulated annealing method, the parameters of a model are randomly perturbed. The change in cost function created by the perturbation is than evaluated to see if the perturbation is accepted or not. As the cost function increases, the possibility of a perturbation being accepted decreases (the temperature of the annealing decreases). The model will iteratively become better (if it converge at all) (Collins and Kuperman, 1992)

Global optimization methods are all very dependent on a fast forward modelling algorithm and a simple parameterization of the model. This is because most of the computer time is spent on a huge amount of forward modelling calculations (Causse, 1998). As computers are getting faster and better, the necessity of keeping the parameterization simple might decline. Global methods are therefore probably the future for solving the seismic inverse problem.

2.3.2 Linearised methods

If the non-linearity between the data and the model is not too strong, it might be possible to linearise the problem. Born approximation is a common way to linearise the problem (or more precisely, linearise the forward modelling that relates the model perturbation with the data perturbation (Chabert, 2007)):

The new model, $\vec{m}$, will be described by a linear combination of a reference model (current model) $\vec{m}_0$ and a perturbed model $\delta\vec{m}$:

$$\vec{m} = \vec{m_0} + \delta\vec{m} \tag{2.6}$$

and the relationship between the data and the model (see equation (2.2))can be re-written as

$$\vec{d} = g(\vec{m}_0 + \delta\vec{m}) \tag{2.7}$$

The non-linear operator can be developed by a Taylor series of 1st order:

$$g(\vec{m}) = g(\vec{m}_0 + \delta\vec{m}) = g(\vec{m}_0) + \left[\frac{\partial g(\vec{m})}{\partial \vec{m}}\right]_{\vec{m}_0} \delta\vec{m} + O(\vec{m}) \tag{2.8}$$

The residuals of higher orders, $O(\vec{m})$, are neglected, and

$$g(\vec{m}_0 + \delta\vec{m}) - g(\vec{m}_0) = \left[\frac{\partial g(\vec{m})}{\partial \vec{m}}\right]_{\vec{m}_0} \delta\vec{m} \tag{2.9}$$

This means that the relationship between the data perturbations, $\delta\vec{d} = g(\vec{m}_0 + \delta\vec{m}) - g(\vec{m}_0)$, and model perturbations can be written as

$$\delta\vec{d} = \vec{J}_0\delta\vec{m} \tag{2.10}$$

where $\vec{J}_0$ is the partial derivative $\left[\frac{\partial g(\vec{m})}{\partial \vec{m}}\right]_{\vec{m}_0}$ called the Jacobian matrix. The relationship between the data and model perturbations is now linear, with $\vec{J}_0$ as the linear operator.

If it is somehow difficult to solve the (above) linearised problem directly, it can be solved iteratively by local optimization methods, i.e. minimising the cost function in steps. Three of the most common local optimization methods are described below.

The gradient method

The gradient method is a method for minimising the cost function and updating the model. The negative gradient of the cost function represents the steepest descent direction, and the cost function can always be reduced by going in this direction (Štekl, 1997). The gradient is described in equation (2.11) below.

$$\nabla_m \vec{E}_0 = \frac{\partial \vec{E}_0}{\partial \vec{m}_0} = \Re\mathrm{e}\left\{\vec{J}^t \delta \vec{d}^*\right\} \tag{2.11}$$

Here, $\vec{J}^t$ is the transposed Jacobian matrix (also called *the Frechét derivative matrix*). This matrix is the partial derivative of the observed data with respect to the model parameters (see equation (2.12))

$$\vec{J} = \frac{\partial \vec{d}_{\mathrm{obs}}}{\partial \vec{m}} \tag{2.12}$$

In the gradient method, the model is updated using equation (2.13).

$$\vec{m} = \vec{m}_0 - \alpha_0 \nabla_m \vec{E}_0 \tag{2.13}$$

$\vec{m}$ represents the updated model, and $\vec{m}_0$ represents the current model estimation. α is the step-length for updating the model. For non-linear problems, the α can be found by a line search technique in the opposite gradient direction (Pratt et al., 1998).

A disadvantage of this standard gradient method is that it converges slowly and that it can be unstable (Ravaut et al., 2004). To improve that, preconditions, regularisation and scaling can be applied.

The Newton method

A pre-condition to the standard gradient method is to include the inverse Hessian matrix in equation (2.13). The equation then becomes:

$$\vec{m} = \vec{m}_0 - \vec{H}^{-1} \nabla_m \vec{E}_0 \tag{2.14}$$

The Hessian matrix is given by equation (2.15):

$$\begin{aligned} \vec{H} = \frac{\partial^2 \vec{E}}{\partial^2 \vec{m}} = \Re\mathrm{e}\left\{ \vec{J}^t \vec{J}^* \right\} + \\ \Re\mathrm{e}\left\{ \left[\left(\frac{\partial \vec{J}^t}{\partial m_1} \right) \delta\vec{d}^* \left(\frac{\partial \vec{J}^t}{\partial m_2} \right) \delta\vec{d}^* \cdots \left(\frac{\partial \vec{J}^t}{\partial m_n} \right) \delta\vec{d}^* \right] \right\} = \vec{H}_\mathrm{a} + \vec{R} \end{aligned} \tag{2.15}$$

$\vec{H}_\mathrm{a}$ is the approximate Hessian matrix, and when inverted, gives a focusing effect to the gradient vector. The $\vec{R}$ term predicts the presence of first order multiple energy in the gradient vector, hence it works as a de-multiple operator (Pratt et al., 1998).

The complete, inverse Hessian matrix is often very large and difficult to calculate. A simpler and more common method is the Gauss-Newton method.

The Gauss-Newton method

The full Newton method involves time consuming inversions of large matrices. Instead of applying the full Hessian matrix, the Gauss-Newton method uses only the approximate Hessian matrix (equation (2.16)) when updating to the next model parameters (equation (2.17)). The $\vec{R}$ term is small and contributes little to the overall solution if the problem is approximately non-linear, i.e. the cost function is already close to the global minimum (Pratt et al., 1998).

$$\vec{H}_\mathrm{a} = \Re\mathrm{e}\left\{ \vec{J}^t \vec{J}^* \right\} \tag{2.16}$$

$$\vec{m} = \vec{m}_0 - \vec{H}_\mathrm{a}^{-1} \nabla_m \vec{E}_0 \tag{2.17}$$

For equation (2.17) to be valid, $\vec{H}_\mathrm{a}$ must be assumed to be invertible. This is often not the case, and a regularisation parameter to the equation must be added. A simple damping term, $\lambda\vec{I}$, where $\vec{I}$ is the identity matrix and λ

is a weighting factor, is therefore used to derive the model update equation (2.18).

$$\vec{m} = \vec{m}_0 - (\vec{H}_\mathrm{a} + \lambda\vec{I})^{-1}\nabla_m\vec{E}_0 \tag{2.18}$$

The higher the value of the weighting parameter λ, the more the Gauss-Newton method approaches the standard gradient method of equation (2.13). The formula can therefore also include a step length parameter, α, as for the gradient method (Sirgue, 2003).

2.4 Conclusions

The problem of estimating a velocity model from seismic data, as to be investigated later in this thesis, is an inverse problem. In this chapter, some of the theories, problems, and possible solutions of the inverse problem have been discussed.

Global methods are probably the future in the search for suitable solutions to the seismic inverse problem, but today they demand too many resources. Methods using local information about the cost function (i.e. the residuals between the data calculated in a current model estimation and recorded data) in order to reduce this misfit, and find a model that describes the observed data are therefore necessary.

Chapter 3

First-arrival traveltime tomography

Traveltime tomography is a classic seismic imaging method. It uses traveltimes as input data for solving the inverse problem, and creating smooth velocity models of the medium. *First-arrival* traveltime tomography is a method that, as the name implies, only uses traveltimes of the first arriving waves as data for the inversion.

In the first part of this chapter, the first-arrival traveltime tomography code used in the second part, section 3.2, is described. This code originates from the PhD of Céline Ravaut (Ravaut, 2003). Some theoretical aspects about the method are also included in this part.

In the second part of this chapter, the method is used to derive a smooth velocity model of the left part of the 2004 BP velocity benchmark model (Billette and Brandsberg-Dahl, 2005).

3.1 Description of the code used in this project

The method used here is an iterative inversion method. The method seeks to minimise the cost function based on linearisation, and local information about the cost function.

An initial model is defined by slowness values, u, on a regular spaced grid. With information about the acquisition setup (i.e. the source and receiver positions) and the current model estimation, traveltimes are computed using a finite difference numerical method. The program uses the Eikonal solver of Podvin and Lecomte (Podvin and Lecomte, 1991) for computing the first-arrival traveltimes in the medium. When the first-arrival traveltimes to all

the grid points in the model are found, rays are back-propagated from the receivers to the source. Ray tracing is needed to construct the Jacobian matrix (3.1), which consists of the partial derivatives of the data (traveltimes) with respect to the model parameters (here the slowness).

$$\vec{J} = \frac{\partial \vec{d}}{\partial \vec{m}} \tag{3.1}$$

When the Jacobian matrix is constructed, the linearised inverse problem, as in equation (3.2), is solved using the least-square algorithm of Paige and Saunders called LSQR[1] (Paige and Saunders, 1982).

$$\Delta \vec{t} = \vec{J} \Delta \vec{m} \tag{3.2}$$

In order to make the inversion more stable, regularisation (see chapter 2) needs to be applied. The equation to be solved can then be written as the linear system in equation (3.3).

$$\begin{pmatrix} \frac{1}{\vec{\sigma}_\mathrm{d}} \frac{\partial \vec{t}}{\partial \vec{u}} \\ \lambda_\mathrm{v} \vec{C}_\mathrm{v} \\ \lambda_\mathrm{h} \vec{C}_\mathrm{h} \\ \epsilon \vec{G} \end{pmatrix} \Delta \vec{m} = \begin{pmatrix} \frac{\Delta \vec{t}}{\vec{\sigma}_\mathrm{d}} \\ 0 \\ 0 \\ 0 \end{pmatrix} \tag{3.3}$$

In equation (3.3), $\vec{\sigma}_\mathrm{d}$ are the uncertainties related to the picking of the first-arrival traveltimes. $\vec{C}_\mathrm{v}$ and $\vec{C}_\mathrm{h}$ are respectively the vertical and horizontal Gaussian smoothing matrices, and λ_v and λ_h are weight parameters relating to the vertical and horizontal smoothing. $\vec{G}$ is the diagonal damping matrix, and ϵ is its related weighting value. If $\vec{G}$ is the identity matrix, the damping will be constant, but variable damping is also possible.

The perturbated model ($\Delta \vec{m}$) is found from equation (3.3), and the updated model ($\vec{m}$) becomes $\vec{m} = \vec{m}_0 + \Delta \vec{m}$, where $\vec{m}_0$ is the initial model.

3.1.1 Characteristics of first-arrival traveltime tomography

First-arrival traveltime tomography is a method that for many years has proven to be stable, and gives good results, even in lateral heterogeneous media (Chabert, 2007). The data-set for the inversion is small (only first-arrival traveltimes), so the method is fast and efficient.

The first-arrival traveltimes are only sensitive to the long wavelengths of the medium (Chabert, 2007). This limits the possible resolution of the final

[1] *L*east *SQ*uare (linear) *R*egression

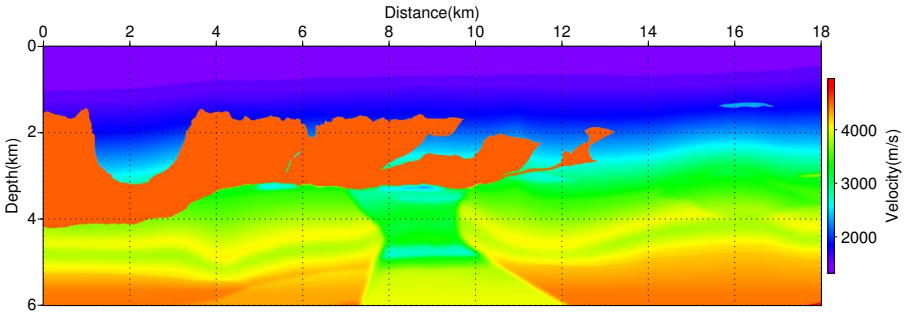

Figure 3.1: The sub-section of the 2004 BP benchmark model that is used for computing the synthetic dataset, and is attempted to be reconstructed by first-arrival traveltime tomography in this section. The model is referred to as "the true model"

estimated model. The resolution is commonly said to be within the width of the first Fresnel zone ($\sqrt{\lambda L}$, where λ is the wavelength and L is the length of the offset range) (Pratt et al., 1996). Another disadvantage with the method is the picking of the first-arrivals from the seismic data. This is both time consuming, and introduces the possibility of picking errors (Improta et al., 2002).

3.2 Application of first-arrival traveltime tomography to the 2004 BP benchmark model

In this part of the chapter, a velocity model is reconstructed from a dataset computed from a sub-section of the 2004 BP benchmark model (Billette and Brandsberg-Dahl, 2005), using the first-arrival traveltime tomography code described in section 3.1. The reduced benchmark model is shown on figure 3.1.

3.2.1 The dataset

When working with real data, the first-arrival traveltimes are identified and picked on the seismic seismograms. In this synthetic test, the "observed data", i.e. the traveltimes used in the inversion, are computed solving the eikonal equation in the true velocity model.

For this test, the considered medium is of 18 km long by 6 km depth. The synthetic acquisition consists of 200 sources and 200 receivers evenly spaced

every 90 meters, covering the medium horizontally from 15 m to 17925 m. Sources and receivers are placed at 15 m depth.

3.2.2 Inversion results

First-arrival traveltime tomography can be used to create starting models for full-waveform inversion (as mentioned in section 3.1.1). However, the final result of the traveltime tomography is also affected by which initial model that is being used. The influence of different starting models, as well as different inversion parameters, have been explored in the search for the model that best represents the true model of figure 3.1.

The initial 1-D velocity model (see figure 3.2(a)) used to produce the final model of figure 3.2(b), is a modified gradient model. The starting velocity of this model is 1500 m/s and the increase is 0.7 m/s per meter. This increase is stopped at 4500 m/s (at a depth of 4200 m). In addition, the seabed topography of the true model was been added to the starting model. This means that the ocean bottom depth is correct in the initial model, and the water column velocity was kept fixed at 1486 m/s during the inversion.

Some of the regularisation parameters, such as the correlation length of the Gaussian filter for smoothing, were modified during the inversion in order to progressively relax the smoothing constraints on the velocity model. The velocities of the model were only allowed to vary between 1480 m/s and 4500 m/s.

The final velocity model (figure 3.2(b)) is obtained after 6 iterations of first-arrival traveltime tomography.

3.2.3 Analysing the inversion result

The RMS error

As mentioned in the beginning of this chapter, the code updates the velocity model on the basis of what minimises the cost function, i.e. provides the best fit between observed and calculated data. The values in figure 3.3 are the RMS values of the residuals between observed and calculated data (=traveltimes). The RMS-values are therefore a measure of how well the calculated data corresponds to the observed data. After the sixth iteration, the RMS-value have been reduced by more than 90 % of the initial misfit, from 210 ms to 18.8 ms. This indicates that the recovered model well describes the observed data. However, if more iterations had been performed, and possibly a greater effort spent on finding the optimal initial model, a better result could have been obtained.

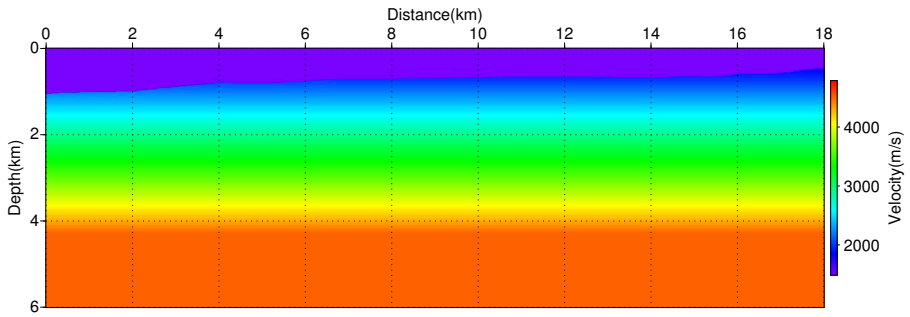

(a) Starting model

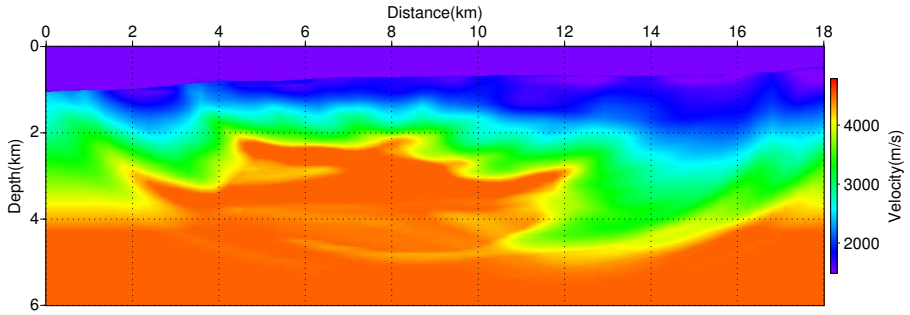

(b) Final model

Figure 3.2: The initial and recovered velocity models

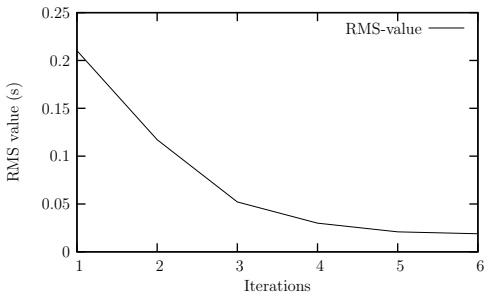

Figure 3.3: RMS value of the data residuals plotted with respect to the number of iterations

Distribution of traveltime residuals

Computing traveltime residuals is another way of quantifying the difference in data fit between the observed data and the data calculated in the model of current interest. This is quite similar to the RMS error, however this analysis shows the distribution of the errors. The distribution of traveltime residuals helps to see if the recovered model is a probable velocity model on the basis of the observed data (Chabert, 2007).

On figure 3.4 the traveltime residuals from both initial and final model are calculated and plotted with respect to the offset distance. This can help tell at which offsets the residuals are large or small, and for which offset ranges the model provides the best traveltime fit. The spread in traveltime residuals have been reduced from the extremal values +0.78 s and -0.43 s in the initial model, to ±0.05 s in the final model. The good gathering of traveltime residuals makes the model a probable velocity model.

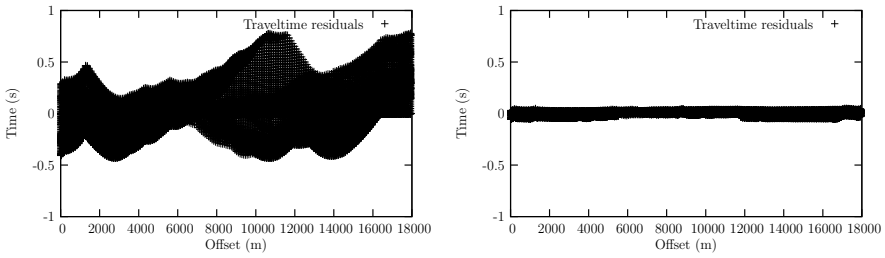

(a) Initial model

(b) Final model

Figure 3.4: Traveltime residuals in initial(a) and final model(b)

3.3 Conclusions

First-arrival traveltime tomography is a stable method for estimating smooth velocity models in heterogeneous media. The method uses little data for the inversion, making it is fast and efficient. However, the resolution is limited because only the large wavelengths of the medium are recovered. First-arrival traveltime tomography can for example be used to determine starting models for full-waveform inversion.

The code used in this study was described and applied to synthetic data from a portion of the 2004 BP benchmark velocity model. The inversion in this example converged well, and the recovered velocity model produced a

first-arrival traveltime misfit of amplitude around 20 ms (RMS-value), i.e. a reduction of more than 90 % from the misfit in the starting model.

Chapter 4

Full-waveform inversion

In this chapter, the theory of full-waveform inversion is presented together with some of the key elements of the code used in the application chapter (Chapter 5). This is also a code originating from the PhD of Céline Ravaut (Ravaut, 2003).

4.1 Introduction

Full-waveform inversion is a method for deriving velocity models from seismic dataset. The velocities are estimated by solving the inverse problem, where the whole wavefield, including waveform and phase, forms the dataset. Because of the large amount of information contained in the dataset, it is possible to create quantitative and high resolution velocity models using FWI (Pratt et al., 1996).

The method was first introduced in 1986 by Albert Tarantola (Tarantola, 1986) in the time domain, and was then extended to the frequency domain by R.G. Pratt in 1990 (Pratt and Worthington, 1990). This master thesis uses the frequency domain FWI. In the frequency domain, the computational cost is only proportional to the number of frequencies used in the inversion, and not the number of sources. If the seismic data contains wide-angle components, there will be a redundancy in the wavenumber spectrum present in the data (Pratt and Worthington, 1990). Such a redundancy can be exploited in the frequency domain FWI by inverting fewer frequencies (and hence save computational costs) because it is possible to invert for single, discrete frequencies one at the time (Ravaut et al., 2004). Another great advantage with the frequency domain implementation is the ease and efficiency when adding multiple sources (which is important in seismic methods) (Štekl, 1997). Both the forward modelling and the inversion are

performed in the frequency domain.

FWI searches for a velocity model that produces a full wavefield that best fit the observed full wavefield. This is generally performed by an iterative local, linearised approach using a gradient method, where each iteration minimises the data residuals (Ravaut et al., 2004). The negative gradient shows the steepest descent direction, i.e. where the data residuals decrease the most. The final model of one iteration provides the starting model for the next iteration (equation (4.1)). Methods based on linearisation of the inverse problem, presents the necessity of an initial model. The seismic inverse problem is practically always non-linear (Chabert, 2007) and the cost function (representing the data residuals) can contain several minima. Since FWI uses a local minimisation method, the starting model should therefore be in the neighbourhood of the global minimum in order to avoid convergence to a local minimum on the cost function.

$$\vec{m}^{(k+1)} = \vec{m}^{(k)} + \delta\vec{m} \tag{4.1}$$

4.2 Frequency domain full-waveform inversion

The objective of FWI is to recover a velocity model that best describes the observed data. This means that a wavefield computed in the estimated velocity model and the recorded seismic wavefield are compared to each other, and the parameters of the velocity model is updated to reduce the misfit between the two wavefields. This process includes forward modelling (computing the wavefield) and solving the inverse problem (estimation of the model parameters). Both of these problems are formulated in the frequency domain in the FWI code used in this master thesis. Some of the key equations in the code are described in this section.

The forward modelling

The forward modelling is, as mentioned, a necessary step when solving the inverse problem. By solving the full time-domain wave equation, the full wavefield can be calculated at any place and any time in the current model. Equation (4.2) is the 2-D acoustic wave equation.

$$\frac{\partial^2 P(x,z,t)}{\partial x^2} + \frac{\partial^2 P(x,z,t)}{\partial z^2} - \frac{1}{c^2(x,z)}\frac{\partial^2 P(x,z,t)}{\partial t^2} = S(x,z,t) \tag{4.2}$$

The wave equation can be obtained in the frequency domain by a simple Fourier transformation of the time-domain equation. The scalar, 2-D fre-

quency domain, acoustic wave equation can hence be written as equation (4.3):

$$\frac{\omega^2}{c^2(x,z)}P(x,z,\omega) + \frac{\partial^2 P(x,z,\omega)}{\partial x^2} + \frac{\partial^2 P(x,z,\omega)}{\partial z^2} = S(x,z,\omega) \tag{4.3}$$

where ω is the angular frequency, c is the velocity, $P(x,z,\omega)$ is the pressure field and $S(x,z,\omega)$ is the source function. Viscous attenuation can be implemented by making the velocity, c, a complex value.

The previous wave equation can be written in the following matrix form:

$$\vec{W}\vec{P} = \vec{S} \tag{4.4}$$

where $\vec{W}$ is a complex impedance matrix ($\vec{W} = \frac{\omega^2}{c^2} + \nabla^2$ where ∇^2 is the Laplacian operator), $\vec{P}$ is the pressure field and $\vec{S}$ is the source function. This system of linear equations (equation (4.4)) can either be solved by a direct or iterative method. In the code, the equation is solved directly by LU factorisation of the impedance matrix, and then forward and backward substitution, as direct methods are very appropriate to solve multi-source problems. The pressure field is computed by an advanced form of the finite difference approximation called *mixed grid approach*. This technique uses a combination of a regular grid and a grid tilted 45°, and describes the pressure at one point as a weighted combination of pressure values from 9 different nodal points. The mixed grid approach ensures an efficient implementation of the wave equation for numerical calculations on a computer. The approach is described in more details by for instance Ivan Štekl (Štekl, 1997).

The inversion problem

The full-waveform inversion code used in this master thesis uses a gradient method to determine what model parameters that will minimise the wavefield residuals, and hence be defined as the best velocity model. The gradient of the cost function includes the Jacobian matrix, which is the partial derivatives of the data (wavefield/pressure field) with respect to the model parameters (as seen in section 2.3.2).

Taking the partial derivative of equation (4.4) with respect to the model parameter m_i on both sides, the result will be equation (4.5), because the source $\vec{S}$ is independent of m.

$$\vec{W}\frac{\partial \vec{P}}{\partial m_i} + \vec{P}\frac{\partial \vec{W}}{\partial m_i} = 0 \tag{4.5}$$

This equation can easily be derived to:

$$\vec{W}\frac{\partial\vec{P}}{\partial m_i} = \vec{f}^{(i)} \tag{4.6}$$

where $f^{(i)} = -\frac{\partial\vec{W}}{\partial m_i}\vec{P}$ is a "virtual" source term (Pratt et al., 1998). Since equation (4.6) is analogous to equation (4.4), it is clear that the partial derivatives (i.e. the Jacobian matrix) can be found by forward modelling.

However, the gradient can be found without the exact computation of the Jacobian matrix. If the equation (4.7):

$$\frac{\partial\vec{P}}{m_i} = -\vec{W}^{-1}\frac{\partial\vec{W}}{\partial m_i}\vec{P} \tag{4.7}$$

(derived from equation (4.6)) is substituted (replacing the Jacobian) into the expression for the gradient (equation (4.8), see more in section 2.3.2), and the source-receiver reciprocity principle is exploited (Pratt et al., 1998), the gradient can be written as in equation (4.9).

$$\nabla_m\vec{E} = \frac{\partial\vec{E}}{\partial\vec{m}} = \Re\mathrm{e}\left\{\vec{J}^t\delta\vec{d}^*\right\} \tag{4.8}$$

$$\nabla_m\vec{E}_i = \Re\mathrm{e}\left\{\vec{P}^{\mathrm{t}}\frac{\partial\vec{W}^{\mathrm{t}}}{\partial m_i}\vec{W}^{-1}\delta\vec{d}^*\right\} \tag{4.9}$$

This latter equation actually represents a multiplication of the forward modelled wavefield $\vec{P}$ and the back-propagated residual field $\vec{W}^{-1}\delta\vec{d}^*$ (where all receivers are joined as one "source" when shooting the back-propagated residual field), i.e. the gradient can be interpreted as the time convolution between the two mentioned fields (Pratt et al., 1998).

In the chapter about general inverse theory, the pure gradient method was described as unstable. The solution was to apply some regularisation parameters, such as the Hessian. The FWI code is actually a form of Gauss-Newton method (see section 2.3.2). This method includes the approximate Hessian matrix in order to stabilise the inversion and speed up the convergence. The Gauss-Newton method requires the computation of the Jacobian matrix, as it is a part of the approximate Hessian ($\vec{H}_{\mathrm{a}} = \Re\mathrm{e}\left\{\vec{J}^t\vec{J}^*\right\}$, see equation (2.16)). The complete formula for the updated model, as used in the master thesis, can hence be written as

$$\vec{m}^{k+1} = \vec{m}^{k} - \alpha(\mathrm{diag}\vec{H}_{\mathrm{a}} + \lambda\vec{I})^{-1}\vec{C}_{\mathrm{m}}\nabla_m\vec{E} \tag{4.10}$$

where the diagonal approximate Hessian, $\mathrm{diag}\vec{H}_{\mathrm{a}}$, provides a scaling effect, $\vec{I}$ is the identity matrix that, together with λ, provides weighting of the approximate Hessian, α is the step-length, $\vec{C}_{\mathrm{m}}$ is a smoothing operator that can be applied to the gradient, and $\nabla_m\vec{E}$ is of course the gradient as in equation (4.9).

4.3 How to apply the method

4.3.1 The dataset

Full-waveform inversion tries to fit the whole computed wavefield to the whole observed wavefield. The wavefield is a physical parameter recorded directly at the receivers. Hence, the data are not exposed for human interpretation that can introduce errors, such as picking of traveltimes.

For frequency domain FWI, the recorded time-domain data (the seismograms) must be transformed to the frequency domain. Each seismic trace is therefore Fourier transformed. One complex number can then be used to describe the frequency spectrum of a seismic trace at a given frequency component. Both waveform and phase of the seismic trace is included respectively as the real and imaginary part of the complex number. Figure 4.1 is an illustration of how the data-set of the full-waveform inversion is put together.

In addition to the description of the data-set above, pre-processing of the data is also necessary.

4.3.2 From low to high frequencies

When in the frequency domain, monochromatic wavefields (containing only one discrete frequency) can be added separately in the inversion process. The low frequencies are more linear related to the model perturbations than the high frequencies (Sirgue, 2003). Therefore the inversion process should start with the low frequency components and progressively add higher frequencies. This will help mitigate some of the non-linearity of the problem, hence increasing the chances of finding the global minimum. It also ensures that progressively higher wavenumbers are recovered (Ravaut et al., 2004).

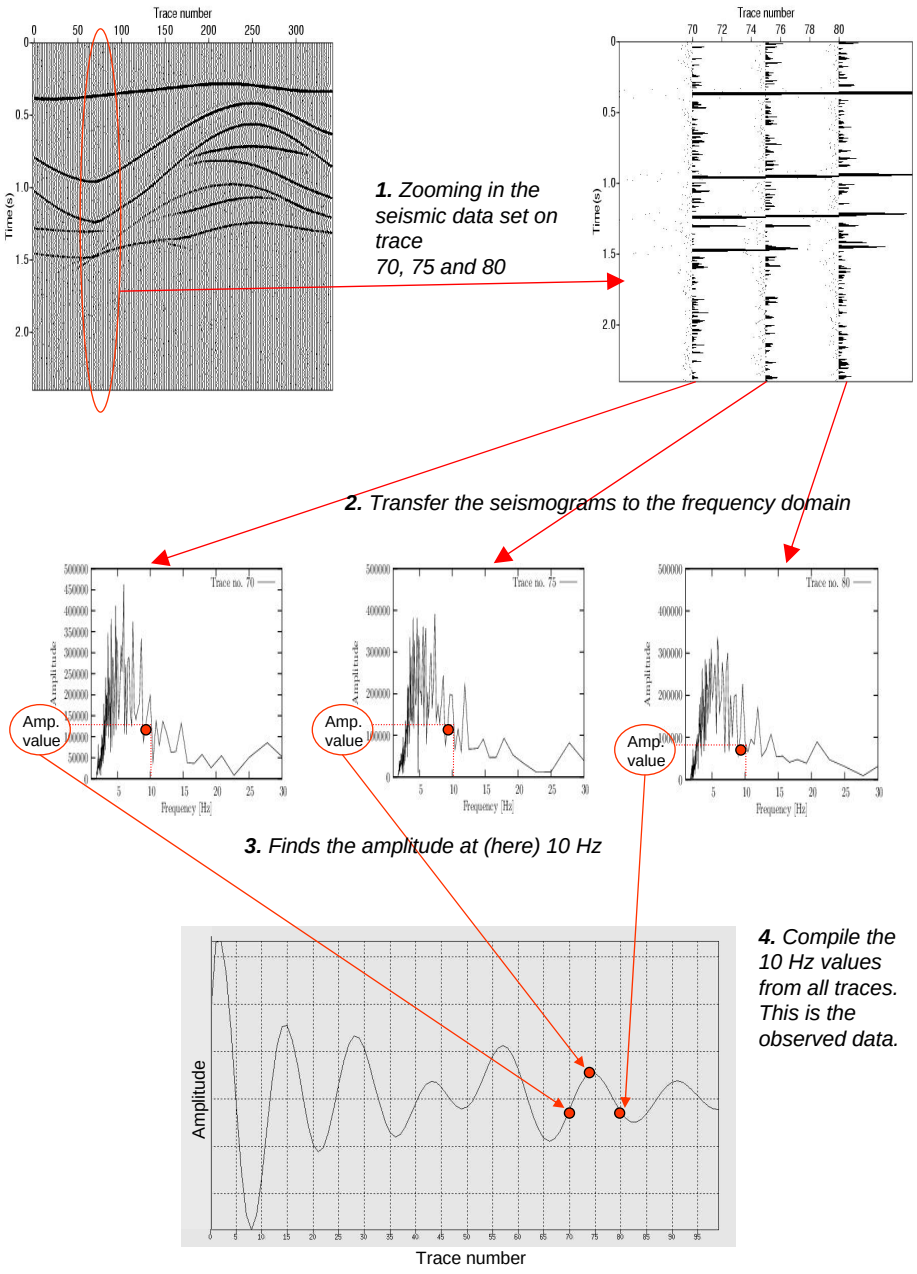

Figure 4.1: The steps (excluding pre-processing) from seismogram to frequency domain data used by the FWI, shown for 3 seismic traces. Each seismogram is transformed to the frequency domain. The values of the frequency spectra at the inversion frequency are compiled together to form the data set. This means that one frequency component of a seismic trace is stored by one complex number

4.3.3 Iterations

The full-waveform inversion method is based on an iterative approach when searching for the velocity model that best explains the observed data. The cost function (representing the data residuals) is minimised at each iteration. The iteration process is non-linear, meaning that the final model of iteration number k serves as the starting model for the next iteration, $k + 1$.

4.4 Other characteristics of the method

4.4.1 Sensitivity to the non-linearity

The seismic inverse problem is a non-linear problem, and the cost function generally contains several minima. Since the method uses a local gradient approach, and not a global search in the model space, the gradient will descend to the nearest minimum on the cost function. It is therefore important that the starting model is in the neighbourhood of the global minimum, so this will be the nearest minimum. A sufficient starting model should be able to produce synthetic data with a misfit to the corresponding arrivals in the observed data of less than half a period of the starting frequency (Sun and McMechan, 1992). Traveltime tomography is a suitable tool for deriving such starting models (Ravaut et al., 2004), however there is no guarantee that the result will be sufficiently accurate. As mentioned, the inversion should start inverting the low frequencies before moving on to higher frequencies. Real seismic sources are bandpass limited, and the lack of low frequencies in the source can be a problem for a real seismic exploration. If the inversion must be started with a higher frequency than desirable, the inversion will have a greater risk of converging towards a local minimum. The recovered model can then explain the wavefield data quite well, but without being similar to the true velocity model.

The regularisation parameters can improve the chances of finding the global minimum. They can also help speed up the convergence.

4.4.2 Resolution

One of the great characteristics of the full-waveform inversion is the high resolution of the results. The method can recover details with an accuracy of $\lambda/2$ (Pratt et al., 1996) (where λ is the wavelength). Compared to traveltime tomography, which can express resolution of approximately $\sqrt{\lambda L}$ where λ is the wavelength and L is the offset range (Pratt et al., 1996), this is a huge improvement.

As much of the wavenumber spectrum as possible should be recovered in a seismic image. The classical approach in seismic imaging have been to first determine the low wavenumbers of the velocity field by velocity analysis, followed by a separate reconstruction of the high wavenumbers. The low wavenumbers provides most of the large scale velocity values (tomography-like contribution), while the higher wavenumbers improves the location and form of the velocities (migration-like contribution) (Mora, 1987). FWI has in theory the possibility to recover the whole wavenumber spectrum during the inversion process (Mora, 1987), hence provide a velocity model where both the velocity values and shapes are accurately estimated.

The Earth can be described as an elastic medium in 3 dimensions. However, the forward modelling in the code used in this master thesis uses, for simplicity reasons and regarding CPU and memory consumptions, a 2-D visco-acoustic wave equation to compute the wavefield. The visco-acoustic approximation includes viscous attenuation, but disregards for instance shear waves.

4.5 Conclusions

Full-waveform inversion can provide a qualitative estimation of the velocities, with good resolution of approximately half a wavelength. The method can recover wavenumbers from the whole wavenumber spectrum, giving accurate estimations on both velocities values and shapes.

The method is very sensitive to the non-linearity of the problem, and a good starting model in the neighbourhood of the global minimum of the cost function is therefore necessary. Inverting from low to high frequencies and applying pre-conditioning factors can also help mitigate the non-linearity of the problem.

All the computations necessary in the method can be performed directly in the frequency domain. The frequency domain implementation has some great advantages regarding the computation cost.

Chapter 5

FWI applied to sub-salt imaging

The main objectives of this master thesis are to evaluate full-waveform inversion applied to a very complex geological structure, and to see if the method can be a useful tool for sub-salt velocity estimations. The model used as a test medium is a sub-part of the 2004 BP benchmark model (as seen on figure 5.1(b)). This is a very challenging medium for seismic imaging, as classical imaging methods usually fails to image in this type of context.

The following sections will investigate the capabilities of the full-waveform inversion, and the conditions that are necessary to recover a satisfactory result in a complex velocity model containing a salt body. First, the full-waveform inversion is applied using a smoothed version of the true model as a starting model. Then, FWI is performed with a starting model derived from first-arrival traveltime tomography. The third section investigates the influence of the number of frequencies that are included in the inversion process. The effect of the starting frequency and initial velocity model are studied at the end of the chapter.

5.1 Presenting the problem

Estimating sub-salt velocities is a difficult challenge. Bodies of salt in the sub-surface generally distort and scatter seismic energy and can create shadow zones where it is hard to retrieve any information (Etgen, 2004). The velocities within a salt body are generally much higher than in its surroundings, and the impedance difference can be large. Hence, a normal problem is noise in the seismograms in the form of multiple reflections between the salt and, e.g. the water layer. In addition, the boundaries of salt

are often complex with many small and sharp variations and steep dips that can be difficult to recover. Normal methods usually fail in this type of context, and especially sub-salt velocities are hard to estimate (Etgen, 2004). The problem of retrieving information below the salt is exposed to a lot of interest, as the salt can be very good traps for hydrocarbons. However, despite the large effort invested in solving the problem, the attempts have been more or less unsuccessful (Singer, 2005).

This master thesis uses a sub-part of the 2004 BP benchmark velocity model as a test medium. The original benchmark model (figure 5.1(a)) was developed especially for complex velocity analysis, because, according to a workshop in 2003 sponsored by EAGE[1] and SEG[2], a salt basin model for synthetic testing was missing (Billette and Brandsberg-Dahl, 2005). The benchmark model can be sub-divided into three parts, each representing a difficult challenge for seismic imaging. The left part of the benchmark model, which is the test medium used in this work, contains a large salt body covering almost the whole length of the medium. This medium represents a typical sub-salt imaging problem, where standard methods have yet to provide stable and good results. The test model is 18 km long by 6 km depth. The salt has a thickness of approximately 2 km, and stretches from 0-13 km along the model. In the middle of the model, below the salt, there is an area (of approximately 8 km^2) of low velocities, representing a low pressure zone. In this zone, two low velocity anomalies can be found at approximately 3.3 km and 4.7 km depth respectively. Such deep and low velocities are very hard to recover. The left part of the benchmark model represents a very difficult, and very non-linear, imaging problem. According to the creators of the model, the main challenges of the left part are: *"obtaining a precise delineation of the salt and recover information on the sub-salt velocity variations "* (Billette and Brandsberg-Dahl, 2005). The left part of the model can be seen on figure 5.1(b), and is referred to as "the true model". The model is specified on a regular square grid of 1201 $\times$ 401 gridpoints. The grid spacing is 15 m.

In the project paper from the fall of 2007 (Thomassen, 2007), a method for deriving background velocity models called *Stereotomography* was tested on the central part of the 2004 BP benchmark model. In this master thesis, first-arrival traveltime tomography have been used to create one of the starting models. The method from the project work has not been applied, because it is not likely to give a satisfying result for the left part of the BP model. Stereotomography is a method based on reflected rays, and the highly complex structure on the salt's upper limit would have scattered the reflections so that little information would have been retrieved. Traveltime

[1] European Association of Geoscientists and Engineers
[2] The Society of Exploration Geophysicists

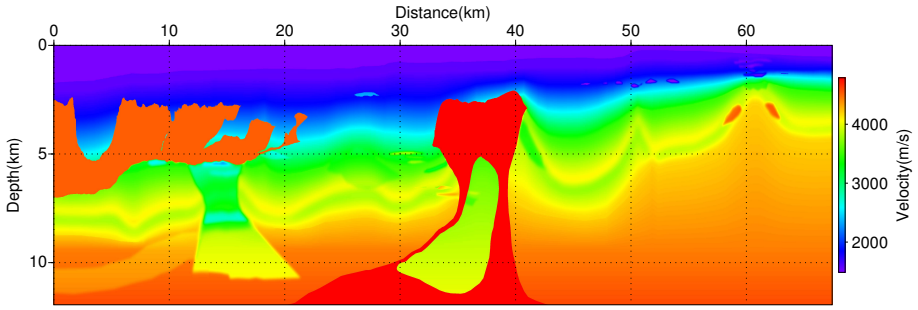

(a) The whole 2004 BP benchmark model

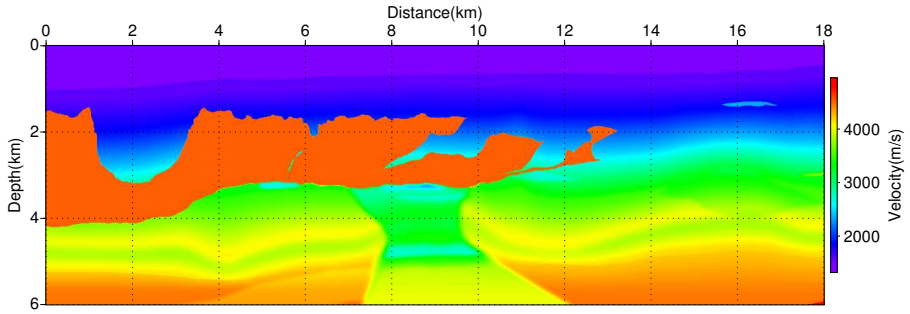

(b) The left part used in this master thesis, i.e. the true model

Figure 5.1: The 2004 BP benchmark models

tomography, using refracted waves, is hence a better choice for deriving a good staring model of the medium in this specific case.

In all applications of FWI in this chapter (except the small test in section 5.6.4 considering the variation of non-linearity with different offsets), the source and receiver acquisition is the same as described in the tomography chapter, 3.2.1: two hundred sources and receivers are horizontally distributed throughout the model, 15 m below the sea surface. The first source/receiver starts at a distance of 15 m from the origin of the model, and the last is located at 17925 m. The spacing between them is 90 m. The source is a Ricker wavelet with a frequency content ranging between 0 and 30 Hz (see figure 5.2(a) and 5.2(b)).

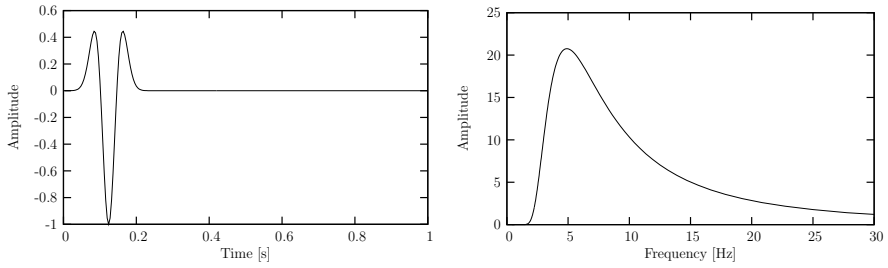

(a) (b)

Figure 5.2: (a) The source wavelet in time domain. (b) The frequency content of the source wavelet

5.2 Application of FWI to derive the sub-salt model

In this section, the process and results of full-waveform inversion are presented. A smoothed version of the true model has been used as a starting model for the FWI.

5.2.1 The Starting model

As FWI is a linearised inverse problem, its results are sensitive to the accuracy of a starting model. In order to avoid cycle-skipping effects, the initial model needs to explain the data within half a wavelength of the lowest available frequencies (Sun and McMechan, 1992). To ensure a satisfying starting model for the FWI, a smoothed version of the true model was chosen in this

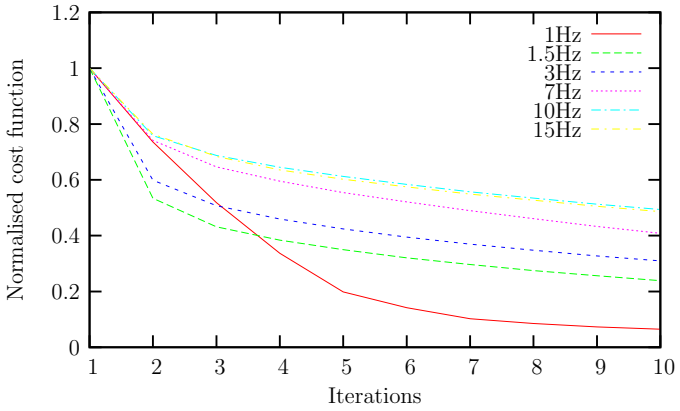

Figure 5.3: Normalised cost function with respect to iterations for a selection of the inversion frequencies

first step. Using the *smooth2* program of the *Seismic Unix toolbox*[3], the true model was smoothed with a smoothing factor of 75[4] in both horizontal and vertical direction. The obtained model is presented as the first model on figure 5.4. The smoothing factor is relatively large, and masks the suddenly high increase of the velocity at approximately 1.6 km depth (see the true model on figure 5.1(b)). It is still possible to recognise a tendency of lower velocities at approximately 3.5 km depth, meaning that the salt body, with its high velocity, is only vaguely outlined. Smoothing the true model ensures a consistent resolution in all parts of the model, even at the sides and at large depths. The smoothed starting model contains the large wavelenght structure of all parts of the true model, but has no sharp velocity variations.

5.2.2 Parameter description

For this first test, 17 frequencies ranging from 1 to 15 Hz were inverted. A variable number of iterations were performed per frequency. The values of the inverted frequencies are presented in table 5.1. The low frequencies were iterated more (20 iterations) than the higher valued frequency components, as the cost function was still decreasing after 10 iterations (see figure 5.3).

According to the gradient and model perturbation formulas from chapter 4, regularisation parameters need to be defined. For this study, these values were:

- λ=0.0001

[3]Seismic Unix is an open source seismic utilities package supported by the Center for Wave Phenomena (CWP) at the Colorado School of Mines (CSM).

[4]Unfortunately, no information on this unit was available

- α=3 %
- $\vec{C}_m$: Not used

λ is a damping parameter for the diagonal approximate Hessian. The value of λ is set quite low (for instance, in (Ravaut et al., 2004), λ was proposed to take values between 0.002 and 0.005, however this is case dependent). This will increase the scaling effect of the Hessian (Pratt et al., 1998) and allow the model to perturb more freely and independent from the starting model. The step-length, α, is set to 3 % of the perturbation value. In addition, no smoothing of the gradient, $\vec{C}_{\mathrm{m}}$, was applied.

Table 5.1: Inversion frequencies and the corresponding numbers of iterations

Frequency	*Iterations*
1 Hz	20
1.5 Hz	15
2 Hz	10
2.5 Hz	10
3 Hz	10
4 Hz	10
5 Hz	10
6 Hz	10
7 Hz	10
8 Hz	10
9 Hz	10
10 Hz	10
11 Hz	10
12 Hz	10
13 Hz	10
14 Hz	10
15 Hz	10

5.2.3 Derived velocity models

The velocity models recovered from FWI are presented on figure 5.4 after the inversion of 1, 3 and 15 Hz frequency component respectively. In addition, the smooth starting model is the upper model on figure 5.4.

From the first two models on figure 5.4, it is clear that after the inversion of 1 Hz, the method has already made large improvements from the starting model. As progressively higher frequency components are included in the inversion process, the resolution of the models increase. Higher wavenumbers can image structures of smaller size. This can be illustrated by the small

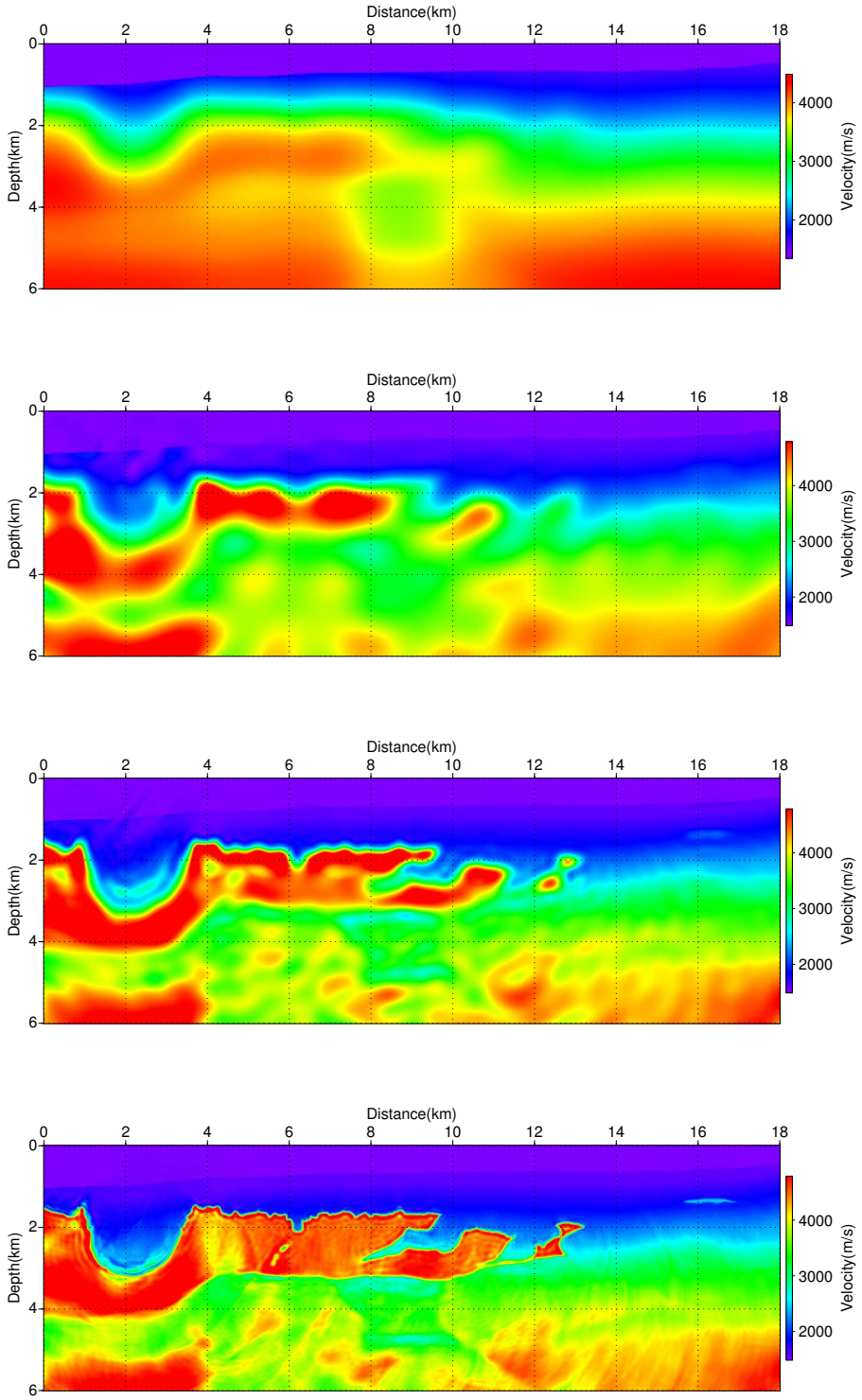

Figure 5.4: Velocity models from top to bottom: Starting model, model after the 1Hz inversion, model after the 3Hz inversion, and model after the 15 Hz inversion

velocity anomaly at the upper right corner. The anomaly is not present in the starting model or the 1 Hz model. At 3 Hz, it is barely noticeable, but in the 15 Hz model, it is completely recovered.

When comparing the recovered model after the inversion of the 15 Hz frequency component (figure 5.4) with the true model (figure 5.1(b)), many similarities can be seen. The salt body is well defined, regarding both location in the model and the boundary details. It is possible to identify details on the (upper) salt boundary with a resolution of approximately 60 m. This corresponds to a resolution in the same order as predicted in the theory (see section 4.4.2), i.e. approximately half a wavelength ($\frac{1}{2}\lambda = \frac{1}{2}\frac{c}{f} \approx \frac{1}{2}\frac{4500\text{m/s}}{15s^{-1}} = 150\text{m}$). The velocities in the deepest third of the model are more inaccurate than in other parts. Especially in the area defined between 4-8 km in horizontal distance and 4-6 km in vertical depth it seems that the velocities are more difficult to estimate. This is just left of the low velocity zone described in section 5.1. However, the general tendencies of the sub-salt velocities have been recovered. It is also very important mentioning that the final 15 Hz model have recovered the low velocity anomalies beneath the salt, at the approximate coordinates (horizontal, vertical): (8.5km, 3.3km), (8.5km, 4.7km) and (5.5km, 3.2km).

5.2.4 Analysing velocity profiles

A more quantified analysis of the velocities is easier when looking at the velocity profiles on figure 5.5. Velocity profiles at three different locations are extracted (at 4005 m, 7995 m and 13005 m) from the true velocity model, the starting model and the recovered model at 15 Hz. In all three figures the estimated velocities above the salt layer matches the true velocities very well. The largest deviation from the true velocity is about 200 m/s in a small area of the 4005 m profile. The transition to the high velocity at around 1.6 km (the upper salt boundary) is almost perfectly recovered in the three velocity profiles. The deepest salt boundary is also recovered very accurate. The full-waveform inversion has managed to "obtain a precise delineation of the salt".

The velocities inside the salt body are of a more varying quality. The 13005 m velocity profile has overestimated the velocity of the thin salt layer with approximately 11 %, or 500 m/s. The 4005 m velocity profile is extracted from an area (4-5 km, 2-3 km) where the recovery of the salt velocities seems to be problematic. The salt velocities of this profile are mainly underestimated, and the maximum deviation is approximately 500 m/s (around 11 %). At the 7995 m profile, the salt velocities are very accurate, only small oscillations differs the estimated velocity from the true velocity. Even velocities from the small (approximately 100 m deep) fracture in the salt at

2.8 km depth, where the velocity suddenly changes from 4500 m/s to 2700 m/s and back to 4500 m/s again, are recovered. This small structure in the very high velocity surroundings would have been impossible to see with for example the first-arrival traveltime method.

Recovery of the sub-salt velocities is one of the most interesting issues concerning the inversion. The transition from the lower salt boundary to the sub-salt part of the model are excellent reconstructed at the 7995 m profile. This sudden decrease in velocity between 3.3 and 3.5 km would neither have been recovered with more classical methods. The rest of the sub-salt velocities in this profile are generally slightly overestimated. In the velocity profile extracted at 13005 m are the sub-salt velocities very accurate down to 5 km depth. The inversion has for example recovered the reduction in velocity between 4.2 and 5 km. The sub-salt velocities from the 4005 m velocity profile seem more inaccurate than the other two profiles, however the lower boundary transition is well recovered. The average velocity difference between the estimated and true sub-salt velocities are approximately 200 m/s, based on the three profiles combined. If the true sub-salt velocities is roughly averaged to 3500 m/s, then this average velocity deviation is only about 6 %.

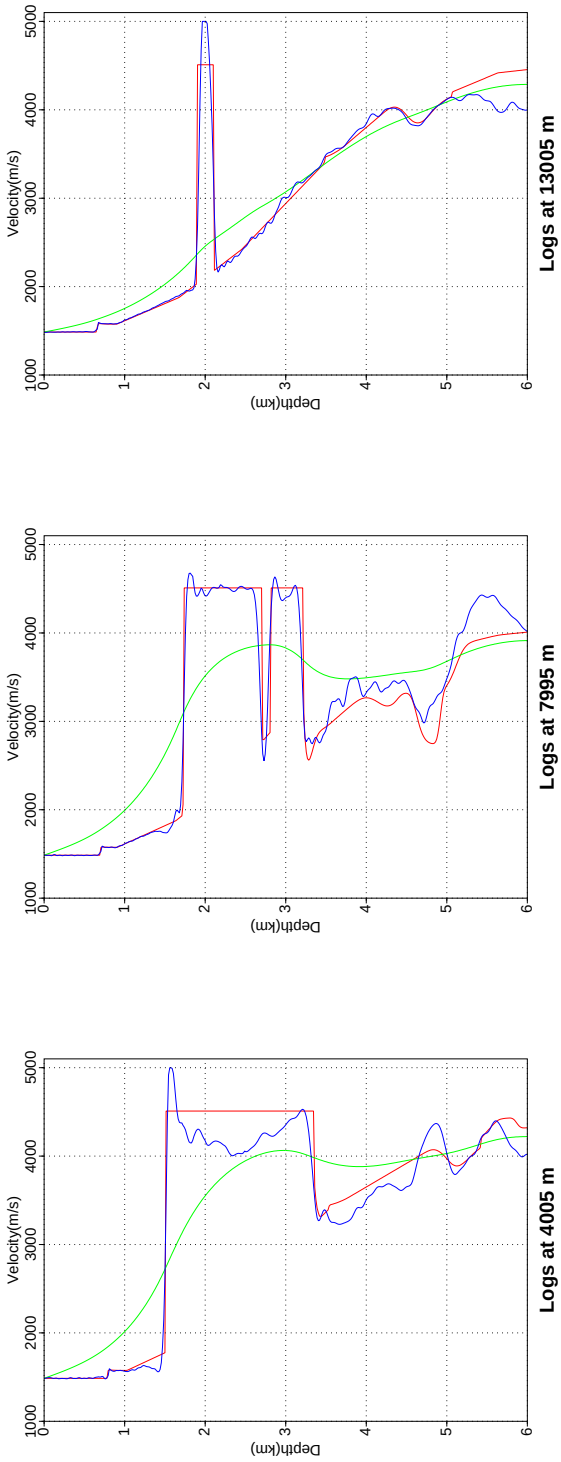

Figure 5.5: Velocity profiles extracted at 4005 m, 7995 m and 13005 m. Red=True model Green=Starting model Blue=Final 15 Hz model

5.2.5 Data fit in the frequency domain

The improvement of the frequency domain data from the starting model and to the final derived model is shown in figure 5.6. Data of 1 Hz frequency component and data of 15 Hz frequency component are computed in the starting model and the final model, so that the data fit for of low and high frequencies can be studied. Both the real and imaginary part of the data are shown. All plots are recordings of shot no. 5, 375 m from the origin of the model. However, while 1 Hz frequency component data are received at all 200 receivers, the 15 Hz frequency component data are only shown for the last 100 receivers (located at 9-18 km).

The data have improved for both the low and high frequency component, and for the real and imaginary part of the data. The final model is (of course) a "better fit model" than the starting model. However, there are still some mismatch between the observed data and the data computed in the final model.

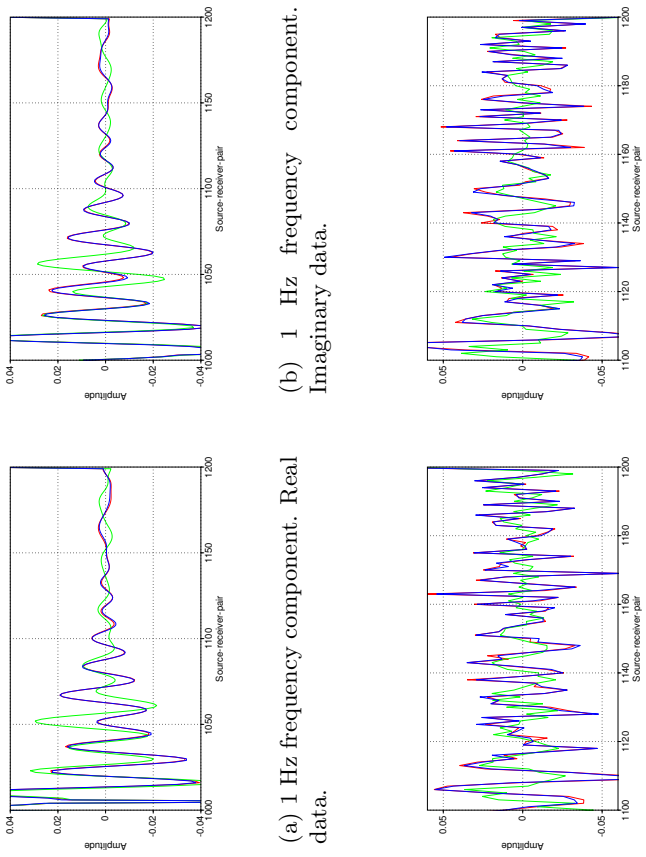

(a) 1 Hz frequency component. Real data.

(b) 1 Hz frequency component. Imaginary data.

(c) 15 Hz frequency component. Real data.

(d) 15 Hz frequency component. Imaginary data.

Figure 5.6: Different data fit plots.Red=Observed data Green=Data computed in the starting model Blue=Data computed in the final model

5.3 Application of FWI using a more realistic starting model

In this section, full-waveform inversion is applied using a starting model derived from first-arrival traveltime tomography. This makes the inversion process more realistic, as starting models for real data experiments must be found using some sort of velocity analysis. First-arrival traveltime tomography methods have been found appropriate for creating such starting models in several papers, for instance in (Ravaut et al., 2004), in (Sirgue and Pratt, 2004) and (Operto et al., 2004).

5.3.1 The starting model

The starting model for this inversion is the first-arrival traveltime tomography model derived in chapter 3. The starting model must be in the "neighbourhood" of the global minimum of the cost function, so that the inversion can converge correctly towards the true global minimum. As mentioned before, this means that the starting model should produce data in the time domain that are less than half a cycle of the starting frequency away from the corresponding observed data. The analysis of the recovered traveltime model showed that the total RMS residual of the model was less than 20 ms (as seen from figure 3.3), and with all first-arrival traveltime residuals less than 50 ms. This should be well within the limits for a starting frequency of 1 Hz, at least for the first arrivals.

The resolution of the derived starting model is not the same in the entire model. The geometry of the acquisition setup and the nature of the rays prevent recovery of information on the sides of the model, especially in its deeper parts. Rays might not have reached the deepest, more central parts of the model the either, making the first-arrival traveltime tomography model less perturbated and more dependent from its own initial model in such areas. It is a potential problem if the velocities in these parts are too far from the true velocities.

The starting model for the FWI in this section is shown on the upper of figure 5.8 (and in chapter 3).

5.3.2 Parameter description

For the FWI to be comparable to the previous FWI using a smoothed starting model, the inverted frequencies and regularisation parameters are the same than section 5.2.

- λ=0.0001
- α=3 %
- $\vec{C}_m$: Not used

However, the number of iterations for each frequency can be different. An overview of the inversion frequencies and corresponding number of iterations are given in table 5.2. The cost function reduction is shown on figure 5.7 for some of the inverted frequencies.

Table 5.2: Inversion frequencies and the corresponding numbers of iterations

Frequency	*Iterations*
1 Hz	20
1.5 Hz	20
2 Hz	20
2.5 Hz	20
3 Hz	15
4 Hz	15
5 Hz	15
6 Hz	15
7 Hz	10
8 Hz	10
9 Hz	10
10 Hz	10
11 Hz	10
12 Hz	10
13 Hz	10
14 Hz	10
15 Hz	10

5.3.3 Derived velocity models

The recovered velocity models from the full-waveform inversion are seen on figure 5.8. This figure presents the starting model, as well as the recovered models after the inversion of 1, 3, and 15 Hz frequency component.

The recovered model after the inversion of 15 Hz frequency component have a great resemblance to the true velocity model. The salt body is well defined both at the top and bottom boundaries, and the velocities are reduced, as they should, beneath the salt. The low velocity reflectors in the low pressure zone, which are very difficult to estimate, are also recovered. However, two areas of the recovered model can clearly be distinguished from the true model: The underestimated velocities at (0-1 km, 2-3 km) and at (4-5 km,

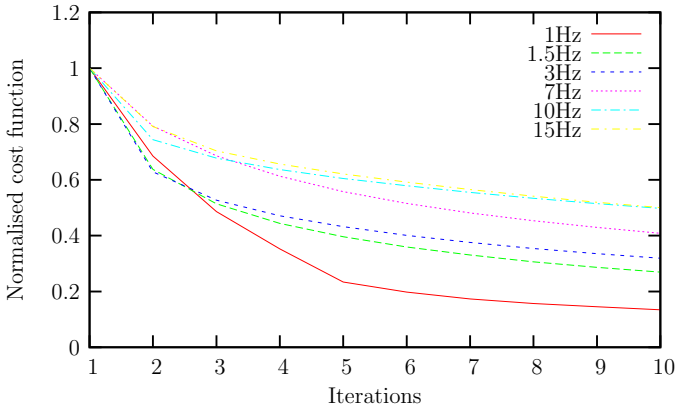

Figure 5.7: Normalised cost function with respect to iterations for a selection of the inversion frequencies

2-3 km). The area around (4-8 km, 4-6 km) does not seem to correspond too well with the true velocities either. This is propably due to erroneous values coming from the initial model.

5.3.4 Analysing velocity profiles

The velocity profiles extracted from the velocity model after the inversion of 15 Hz frequency component, using the initial model from first-arrival traveltime tomography, are shown on figure 5.9.

The velocities extracted at 4005 m have recovered the transition to the salt at approximately 1.6 km depth practically perfectly, and the velocities above this depth are also very good. The velocities between 1.6 and 3.5 km depth differ more from the true velocity logs. The velocities in this area are changing between being over and underestimated. The sub-salt velocities in this profile, are approximately $\pm$100 m/s from the correct velocity down to around 4.5 km (which is roughly a 3 % deviation from the true velocities). From this depth on, the estimations are getting slightly worse, and the difference increases to roughly 400 m/s, which an overestimation of about 10 %.

At 7995 m, the only differences between the recovered and true velocity profiles down to approximately 3.3 km are some minor oscillations. The drop of velocities at 2.8 km are even better recovered here than the for very good inversion result in 5.2. Below this depth, the velocities are generally overestimated. The deviations are at some places as high as 1000 m/s. The shape of the profile in these depths is, however, very similar to the shape of the true velocity profile. This includes a significant velocity reduction at around 3.5 km and 4.7 km representing the two low velocity anomalies

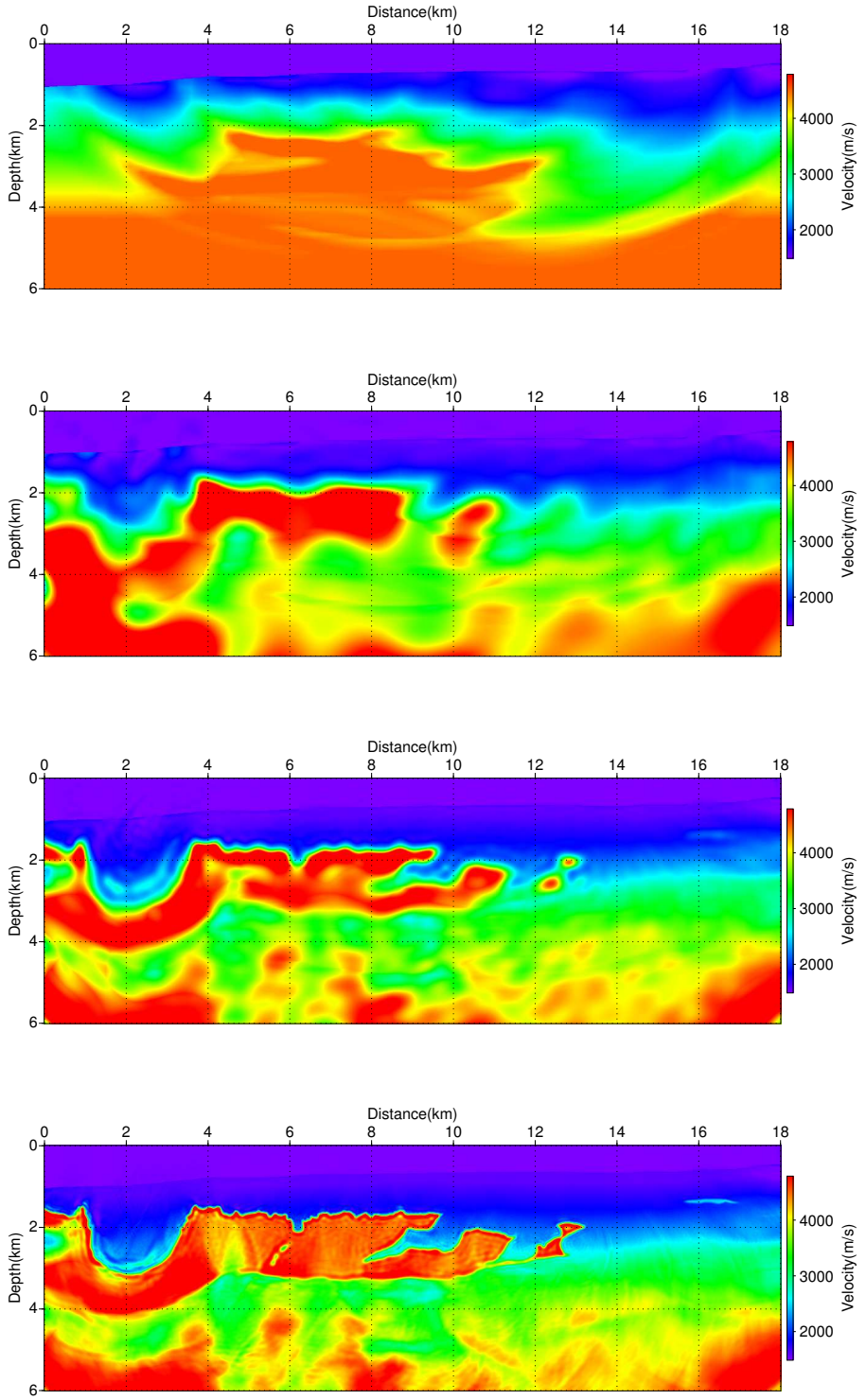

Figure 5.8: Velocity models from top to bottom: Starting model, model after the inversion of 1Hz, model after the inversion of 3Hz, and model after the inversion of 15 Hz

mentioned earlier. The starting model at this distance has sub-salt velocities far from the true model. The initial model has a velocity of 4500 m/s all the way from around 2.5 km depth and throughout the model. Hence, the differences to the true velocities are sometimes more than 2000 m/s (or roughly 70 %) overestimated, which is a substantial gap for the FWI to try to recover. Since the shape of the profile in the sub-salt part is roughly the same as the true profile, the general overestimation is coming from the initial model. If the first-arrival traveltime model had been improved in these areas, the final result after FWI would also have been better.

The last velocity profile is extracted at 13005 m. At this distance the velocities are well recovered throughout the model. The maximum deviation from the true velocity profile is (disregarding the overestimations in the salt) around 200 m/s (5 %), but this deviation occurs only at a few depths. The maximum salt velocity is overestimated with 500 m/s, but the top and bottom salt transitions at 1.8 and 2.2 km respectively, are perfectly recovered.

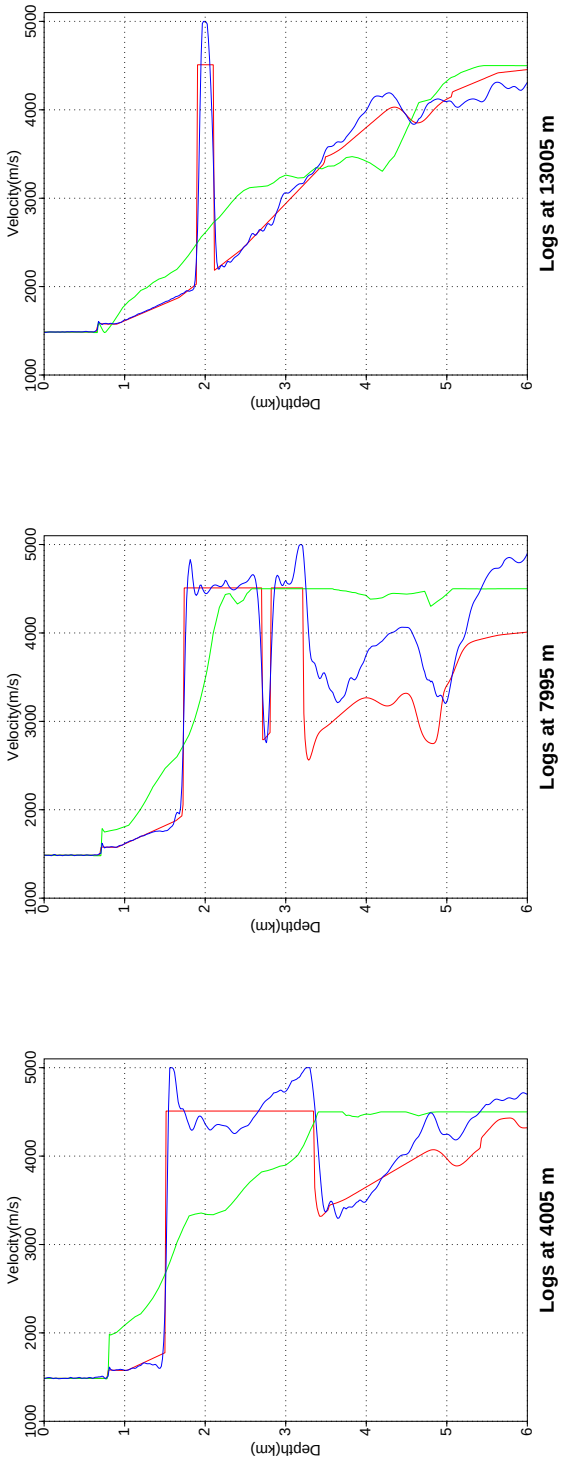

Figure 5.9: Velocity profiles extracted at 4005 m, 7995 m and 13005 m. Red=True model Green=Starting model Blue=Final 15 Hz model

5.3.5 Data fit in the frequency domain

On figure 5.10 are the data computed in the starting model, the data computed in the final model and the observed data plotted, with green, blue and red colour respectively. The data are computed for the 1 Hz frequency component and the 15 Hz frequency component. Both real and imaginary part of the data are shown. The outtakes are, as in section 5.2.5, from the source at 375 m and recorded at all 200 receivers for the 1 Hz frequency component, and the last 100 receivers for the 15 Hz frequency component.

It is easy to see that the final model describes the observed data much better than the starting model. The data from the final model are very similar to the observed data for both low and high frequencies.

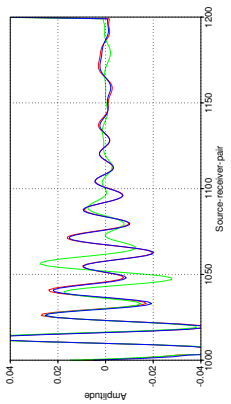

(a) 1 Hz frequency component. Real data.

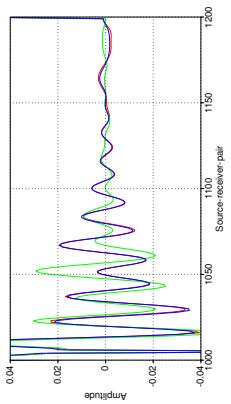

(b) 1 Hz frequency component. Imaginary data.

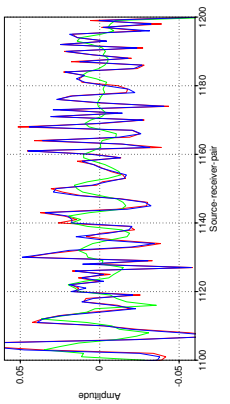

(c) 15 Hz frequency component. Real data.

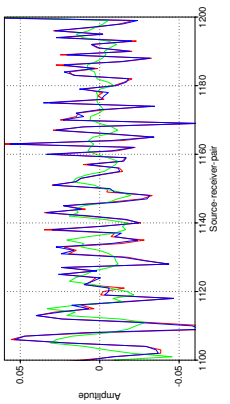

(d) 15 Hz frequency component. Imaginary data.

Figure 5.10: Different data fit plots.Red=Observed data Green=Data computed in the starting model Blue=Data computed in the final model

5.4 Influence of the number of frequencies inverted

How to choose the frequencies for a frequency domain full-waveform inversion is a challenging problem without a clear answer. According to the Nyquist-Shannon sampling theorem, the step length of the frequencies should not exceed the inverse of the cycle duration ($\Delta f \leq \frac{1}{T}$). This is a general rule in signal processing to avoid aliasing. However, multiple papers have shown that for FWI, an un-aliased image can be recovered with the use of fewer frequencies (Sirgue and Pratt, 2004).

In a good seismic image, as much as possible of the wavenumber spectrum should be recovered. Traditionally, velocity analysis provided the low wavenumbers, and migration the high wavenumbers of the seismic image. The low wavenumbers control the large scale velocity distribution of the image and the higher wavenumbers control the smaller wavelengths in the image (Mora, 1987), i.e. reflectors or interfaces. Low frequencies have a more linear relationship to the low wavenumbers. To be able to recover the low wavenumbers, and hence the true velocities, it is necessary to include low frequencies in the inversion at an early stage (Sirgue and Pratt, 2004). However, it is not necessarily the low frequencies of the source that provides the low wavenumbers in the recovered image (Mora, 1987), the wavenumbers can also be defined by the acquisition geometry, i.e. the offsets ranges (Ravaut et al., 2004). Indeed, a spatial wavenumber, $\vec{k}$, is defined by the following equation:

$$\vec{k} = \omega \vec{q} \tag{5.1}$$

where ω is the angular frequency, and $\vec{q}$ is a vector related to the aperture of the acquisition. Large offsets gives a smaller $\vec{q}$ (and smaller wavenumbers), and short offsets gives bigger $\vec{q}$ (and higher wavenumbers).

5.4.1 "Efficient waveform tomography"

In his PhD (Sirgue, 2003), Laurent Sirgue presented a formula for selecting the inversion frequencies. The strategy is based on a 1-D homogeneous assumption of the medium, and the main idea is that larger offset data creates redundant information in the wavenumber spectrum. If the inversion frequencies are carefully selected to avoid redundant information in the wavenumber spectrum, fewer frequencies are needed in the inversion. The larger the offsets, the fewer are the frequencies necessary to recover a continuous wavenumber spectrum. The strategy is also presented in an article by Sirgue and Pratt (Sirgue and Pratt, 2004), were it is named "efficient waveform tomography". The formula is tested in the next paragraphs, to

see if the FWI can be performed more efficiently in this complex medium, and to examine the effects when fewer frequencies are used in the inversion.

5.4.2 The starting model

In these next paragraphs, FWI will be applied to the complex true model with the strategy for selecting the inversion frequencies developed by Sirgue (Sirgue, 2003). The starting model for this test is the smoothed true model, i.e. the same starting model as for the first application in section 5.2. It will thus be possible to compare the final result from this "efficient inversion" with the velocity model derived by the more comprehensive inversion process.

5.4.3 Parameter description

According to (Sirgue, 2003), the inversion frequencies, f, can be selected by equation (5.2). This formula ensures, theoretically, the recovery of a continuous wavenumber spectrum, but without redundant information.

$$f_{n+1} = \frac{f_n}{\alpha_{\min}} \tag{5.2}$$

where

$$\alpha_{\min} = \frac{1}{\sqrt{1 + \left(\frac{h_{\max}}{z}\right)}} \tag{5.3}$$

and $h_{\max}$ is the maximum half offset range available, and z is the depth.

For the true model, the half offset distance, h, is 9 km, and the depth, z, is 6 km. Equation (5.2) hence give a selection of frequencies presented by table 5.3, when the starting frequency is 1 Hz.

Table 5.3: Inversion frequencies and the corresponding numbers of iterations

Frequency	*Iterations*
1 Hz	20
1.8 Hz	15
3.3 Hz	15
5.9 Hz	15
10 Hz	15
15 Hz	15

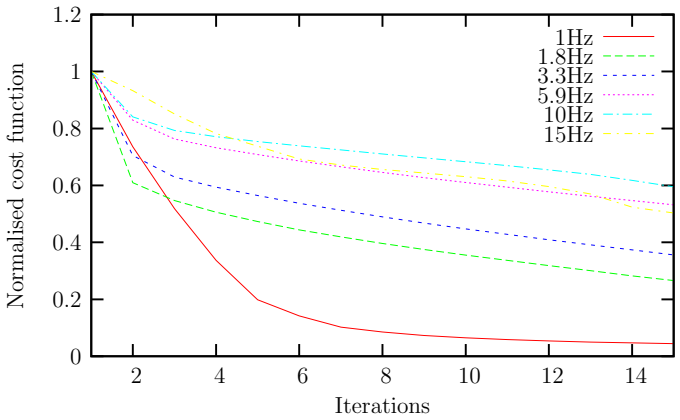

Figure 5.11: Normalised cost function with respect to iterations, for all frequencies included in the inversion process

The inversion is stopped at 15 Hz, and not 19.8 Hz as the formula would have predicted, so that the final results are more comparable to the inversion in section 5.2 (where 15 Hz was the highest inversion frequency). The number of iterations at each frequency component is increased compared to the inversion in section 5.2, however the total number of iterations is still much lower (95 vs. 165). The decrease of the normalised cost function with respect to iteration number is shown on figure 5.11. The regularisation parameters are the same as in section 5.2:

- λ=0.0001
- α=3 %
- $\vec{C}_m$: Not used

5.4.4 Derived velocity models

The recovered velocity models derived from FWI using the sparse selection of frequencies are shown on figure 5.12. The models are chosen so that they can be compared to figure 5.4.

The efficient FWI only included 6 frequencies in the inversion, compared to 17 frequencies for the inversions in the previous sections. This will of course save computation time, but the result does not seem to be quite as good. The velocities in the salt body seem too low, and the salt boundaries are not very distinguished. The low velocity zone below the salt is not as defined as in the true model. The reconstructed model also fails to present some of the details, like the two small “holes” in the salt at (5.6-6 km, 2.5-2.9 km).

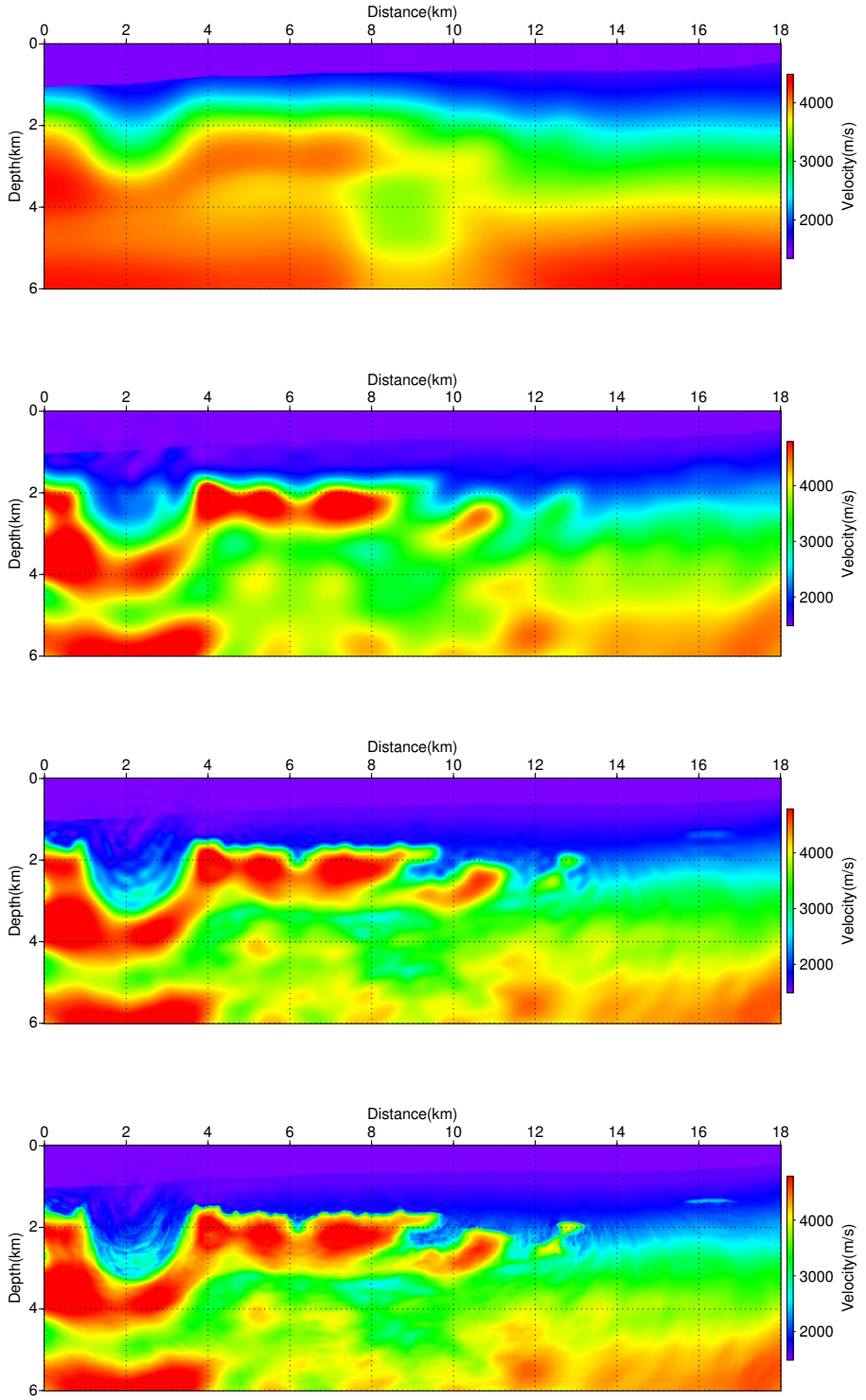

Figure 5.12: Velocity models from top to bottom: Starting model, model after the inversion of 1Hz, model after the inversion of 3.3Hz, and model after the inversion of 15 Hz

5.4.5 Analysing velocity profiles

The velocity profiles (figure 5.13) confirm the indications from the reconstructed model on figure 5.12. The salt body is not well recovered. The transitions between the salt and the surroundings are not as defined as they should. For instance, while the true model increases the velocity from 2060 m/s to 4510 m/s in only 15 m for the upper salt boundary at the 7995 m velocity profile, the recovered model uses approximately 300 m on the same transition. The velocity reduction at 2.8 km are not recovered either.

The sub-salt velocities are somewhat better than the velocities estimated in the areas corresponding to the salt body. At the 4005 m velocity profile, the sub-salt velocities are roughly 400 m/s underestimated from 3.5 to 5 km depth. From just below the salt and down to 4.5 km depth, is the 7995 m velocity profile very similar to the true velocity profile, except for some minor oscillations. The shape from 4.5 km to 6 km are also very similar to the true velocity profile. The low velocity anomaly at around 4.7 km is however not very noticeable in the profile. For the 13005 m velocity profile, the sub-salt velocities are well estimated down to around 4.7 km. Based on these three profiles, the average sub-salt velocity deviation from the true sub-salt velocities is roughly 6-8 %.

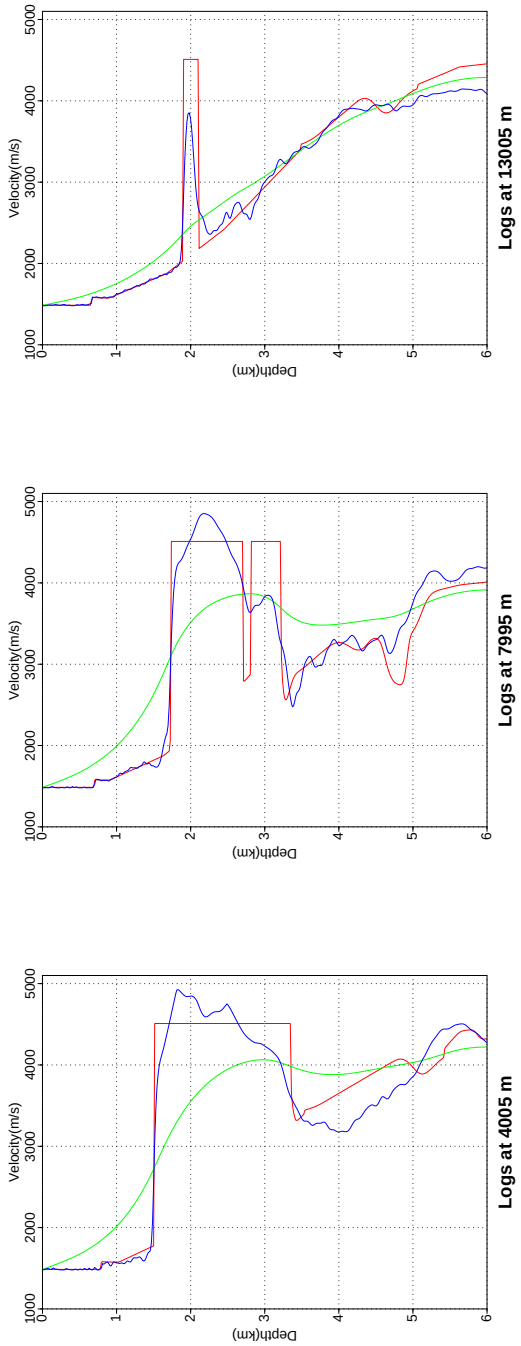

Figure 5.13: Velocity profiles extracted at 4005 m, 7995 m and 13005 m. Red=True model Green=Starting model Blue=15 Hz model

5.4.6 Data fit in the frequency domain

As for the two previous sections, the data computed in the starting model (here the smoothed version of the true model) and the data computed in the final model (as seen on the bottom of figure 5.12) are compared. Figures 5.14 and 5.14(b) represents respectively the real and imaginary part of the 1 Hz frequency component data. Figures 5.14(c) and 5.14(d) represents respectively the real and imaginary part of the 15 Hz frequency component data. The source is located at 375 m, and the receivers are ranging between 0 and 18 km for the 1 Hz frequency component data, and between 9 and 18 km for the 15 Hz frequency component data.

Even though this velocity model was not considered as good as the recovered velocity models in section 5.2 and 5.3, the data of the final model still have a better fit to the observed data than the smoothed starting model. For the low frequency, the recovered model provides a good fit to the observed data. However, the high frequency data are not well fitted to the observed data. This implies that the smaller details are inaccurate in the recovered velocity model. This corresponds with the findings in section 5.4.5, where the sharp velocity transitions were not well recovered. The poor data fit might also mean that more iterations should have been performed.

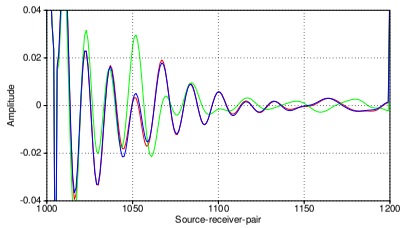

(a) 1 Hz frequency component. Real data.

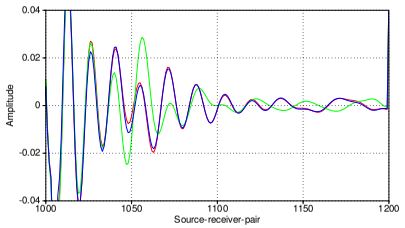

(b) 1 Hz frequency component. Imaginary data.

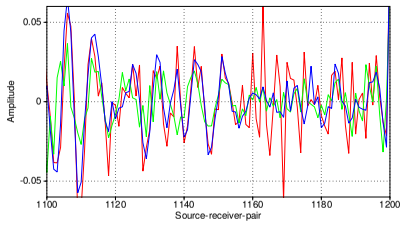

(c) 15 Hz frequency component. Real data.

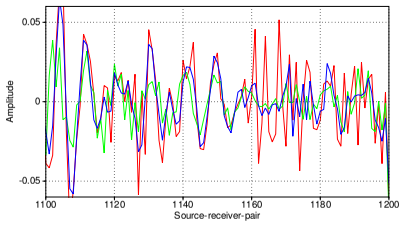

(d) 15 Hz frequency component. Imaginary data.

Figure 5.14: Different data fit plots.Red =Observed data Green=Data computed in the starting model Blue=Data computed in the final model

5.5 Comparing the results from the three full-waveform inversions

In this section, the final reconstructed models from sections 5.2, 5.3 and 5.4 are compared directly to each other. This will give a better idea on whether or not the inversions were successful, and what the three FWI have been able to recover in each case.

The model recovered from the smoothed starting model in section 5.2 is referred to as *"the first model"*, the model recovered from the starting model obtained by first-arrival traveltime tomography is referred to as *"the second model"*, and finally, the model recovered using only six frequency components in the inversion process is referred to as *"the third model"*.

The comparison is performed between the velocity models recovered after the inversion of the 15 Hz frequency component.

5.5.1 The velocity models

The first model and the second model, in figure 5.15, are very similar in the shallowest 2/3 of the model. The velocities above the salt seem well recovered, and so does the salt body itself. The low velocity zone (the area around (7-10 km, 3-6 km)) are better defined and delineated in the first model. In general, the velocities seem more accurate for parts deeper than than 4 km in the first model.

The third model is clearly not as good as the first model, even though they are obtained from the same starting model. The velocity model reconstructed using six frequencies is more "blurred" than the more comprehensive inversion from section 5.2. Fewer details are recovered, and the salt body is less delineated. The low velocity zone beneath the salt body is significantly less distinguished. The sub-salt velocities seem to be generally less accurate.

It is also an interesting point that this velocity model is significantly more similar to the 3.3 Hz component model (see the bottom two models on figure 5.12), than the other two models (the first and second model) are compared to their velocity model recovered at 3 Hz (see the bottom two models on figure 5.4 and 5.8 respectively). This implies that the third model has improved less than the first and the second model from the inversion of the 3 Hz component to the inversion of the 15 Hz component. It is possible that the result of the third model would have been better if it had been iterated even more.

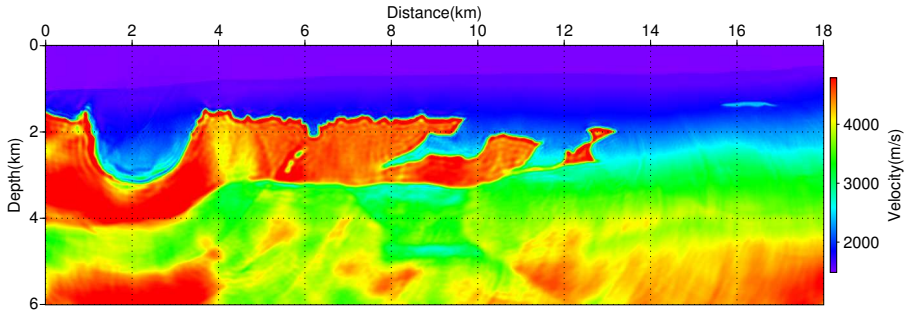

(a) The result using a smoothed version of the true model as starting model

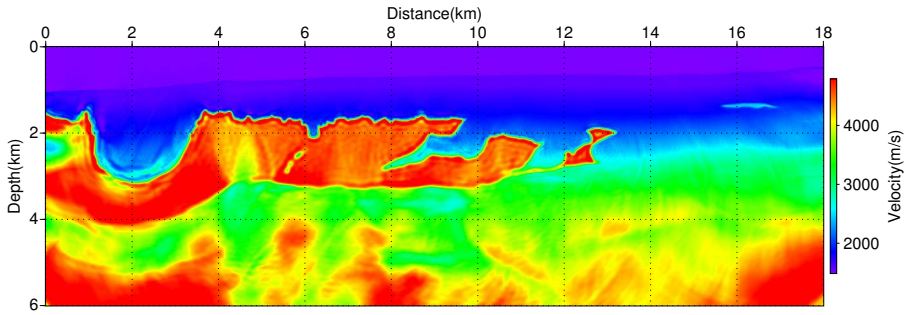

(b) The result using a starting model derived from first-arrival traveltime tomography

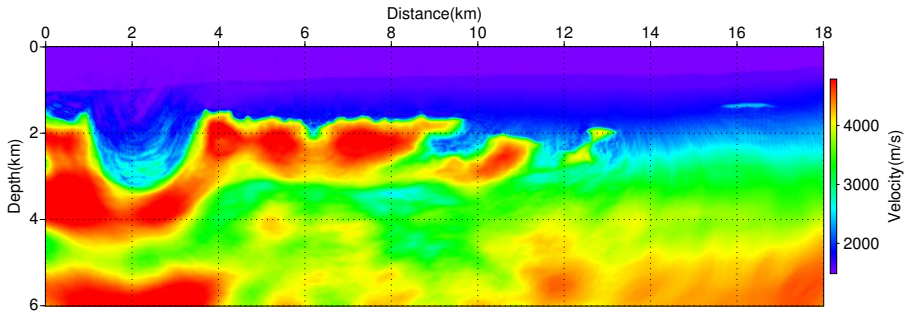

(c) The result using a smoothed version of the true model as starting model, but only six inversion frequency components are inverted

Figure 5.15: The three final models to be compared

5.5.2 The velocity profiles

The velocity profiles from the true model and the three recovered models are directly compared to each other on figure 5.16. The velocity profiles extracted from the first and second model, are very similar at all distances (4005, 7995 and 13005 m). The differences are best seen sub-salt, where the smoothed starting model has provided a much better basis for the inversion. However, both inversions must be considered successful in recovering much of the sub-salt velocities, and estimating the sudden velocity transitions at the salt boundaries.

The third model is less accurate than the comprehensive inversion model from section 5.2, at least down to around 3.5 km depth. Smaller details and sudden transitions are absent in the velocity profiles of the third model. The sub-salt velocities seen on the profiles at 7995 and 13005 m are approximately as good as for the first model, while at the 4005 m profile, the third model represents a larger deviation from the true sub-salt velocities. The main contrasts are seen in the profile, but the less details are recovered.

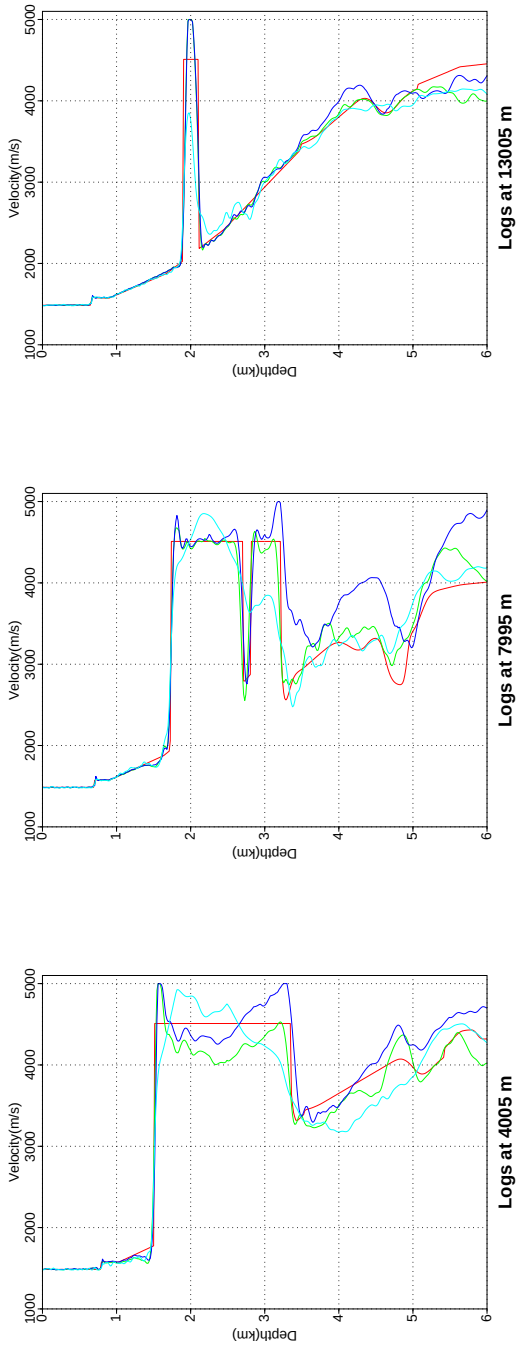

Figure 5.16: Velocity profiles extracted at 4005 m, 7995 m and 13005 m. Red=True model Green=The first model Blue=The second model Cyan=The third model

On figure 5.17, the average velocity differences between the three recovered velocity models and the true velocities are plotted as a function of the horizontal distance in the model, i.e. the average velocity differences are calculated on the basis of extracted velocity profiles at 795, 1995, 4005, 5700, 7995, 10005, 12000 and 13005 m. In figure 5.17(b), 5.17(c) and 5.17(d), the true model has been separated in three parts: above salt, in salt and sub-salt respectively. These three plots will hence present an overview of which parts of the models where the velocities are well estimated. Figure 5.17(a) represents the total average velocity difference calculated over the entire model depth. The average differences are absolute values, meaning that both over and underestimated velocities will positively add to the difference.

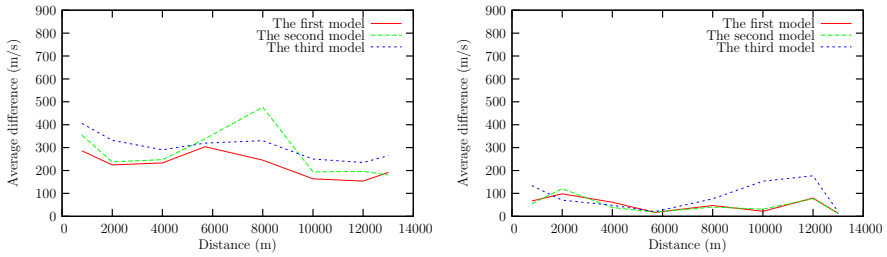

(a) Total differences

(b) Differences above salt

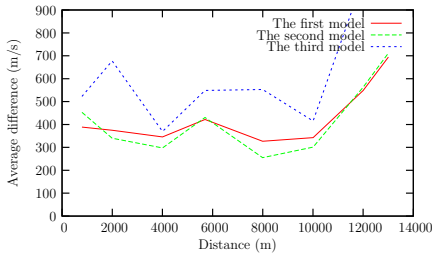

(c) Differences in salt

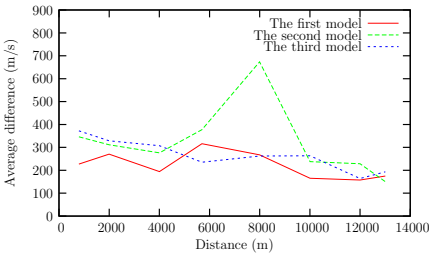

(d) Sub-salt differences

Figure 5.17: Average velocity differences between recovered and true velocity profiles

It is clear from the plots on figure 5.17 that the velocities are best estimated in the shallowest part of the models, i.e. above the salt. The differences are less than 50 m/s for the first and second models in the central parts, whereas the third model has some larger differences, especially between 6 and 12 km. A 50 m/s difference is less than 5 % from the true velocities.

The velocities at the depths corresponding to the salt body, have the overall highest velocity differences (figure 5.17(c)). This is also the part of the

model where the true velocity is the highest (4510 m/s), so the deviation in percentage is only around 10 % for a difference of 400 m/s (which is roughly the deviation of the two first models). The velocity model recovered with only 6 frequency components, has a much higher deviation than the other two. The average difference from the true model velocities varies from 400 m/s and up to more than 1100 m/s. It is clear that the third model have difficulties estimating the velocity of the salt (as already seen in the model and velocity profiles).

The large differences in the "salt part" of the model compared to the two other parts, may be affected by the velocity transitions between the salt structure and the surroundings. These are included when calculating the differences in this part of the model. Even though the estimated velocities seem to follow the true velocity almost exactly in these parts, a barely smoother transition than the sudden true transition can result in large deviations when calculating the velocity mismatch.

The sub-salt parts of the velocities (figure 5.17(d)), express the largest differences between the velocities extracted from the models recovered using the smoothed starting model, and the velocities extracted from the velocity model recovered by first-arrival traveltime tomography. The sub-salt velocities are most inaccurate for this latter model. The first model generally represents the best sub-salt velocity estimations. The second model has a peak in the velocity differences at approximately 6-10 km. In these parts, the deviation increases to as much as 700 m/s, while the velocity differences in the rest of this model are between 200-400 m/s. In the third model, the sub-salt velocity differences are fairly stable around 200-400 m/s.

If the high, average velocity deviation for the second model between 6 and 10 km is disregarded, the recovered sub-salt velocities for all three models represents a deviation from the true velocities of approximately 200-400 m/s. Because of the large span in the true sub-salt velocities (from around 2200 m/s to 4500 m/s), a 200-400 m/s difference can represent a percentage deviation between 4 and 18 %. However, as found in the three previous sections (sections 5.2, 5.3, and 5.4 respectively) the average sub-salt deviation is around 6 % for the first model, 10 % for the second model and 8 % for the third model.

5.5.3 Comments on the reconstruction of "the second model"

It is clear that the starting model has an impact on the final results. Both velocity models derived from the smoothed starting model estimated the sub-salt velocities better than the model derived from first-arrival traveltime tomography. This starting model was inaccurate in the deeper parts of the

model. However, FWI improved the sub-salt velocities significantly from the first-arrival traveltime tomography model.

In the starting model of the second model (as seen as the upper model on figure 5.8), the general reduction of the true velocities below the salt have not been recovered by the first-arrival traveltime tomography. The velocities are very high in the deep parts of the model (around 4500 m/s). The lower, sub-salt velocities are however present in final, recovered velocity model (figure 5.15(b)). This means that the FWI process has recovered the low sub-salt velocities by itself. FWI is capable of recovering low velocities beneath a layer of high velocity, even if these lower velocities are not included in the starting model.

Ray based methods, such as first-arrival traveltime tomography, are unable to estimate such low velocity zones due to the nature of the ray paths. The rays follow Fermat's principle of taking the path of shortest time, and will avoid a low velocity area. Since FWI can recover low velocities in the deeper parts by itself, first-arrival traveltime tomography is not prevented from providing starting models for the FWI.

5.5.4 Comments on the reconstruction of "the third model"

The efficient FWI from section 5.4 with inversion of only a few, carefully selected frequencies did not recover a satisfying result when applied to the complex 2004 BP benchmark model. The final reconstructed velocity model failed to estimate the salt transitions properly, and did not estimate some of the important details of the true model. The theory behind the frequency selection is, as mentioned, based on the assumption of a 1-D homogeneous medium. The 2004 BP model is however a very complex 2-D heterogeneous medium. The low wavenumbers are very important in order to find of the true velocity perturbation. The failure of finding the true velocities in some parts of the model indicates that too few low wavenumbers were recovered. The failure of recovering smaller details, such as the sudden velocity decrease at 2.8 km in the 7995 m velocity profile, indicates that the slightly higher wavenumbers are not recovered properly either.

The vertical wavenumbers are, according to (Sirgue and Pratt, 2004), recovered by the equation

$$k_z = 2k_0\alpha = 2\frac{\omega}{c_0}\alpha \tag{5.4}$$

where k_z is the vertical wavenumber, k_0 is the wavenumber defined by the angular frequency ω and the constant velocity in the homogeneous medium c_0. α is the same as in equation (5.3).

Equation (5.4) indicates that lower wavenumbers are more difficult to recover in the deeper parts of the model (because α will increase when the half offset-to-depth ratio ($\frac{h}{z}$) decreases with larger depths). A proposed solution to this problem (Sirgue and Pratt, 2004), have been to decrease the maximum offset when calculating the frequencies in equation in equation (5.2). This "trick" decreases the value of α and hence increases the number of inversion frequencies. This was proven successful when applied to the Marmousi model[5] in (Sirgue and Pratt, 2004). However, more wavenumbers can just as easy be added by including more inversion frequencies, i.e. adjusting the ω instead of the α in equation (5.4), as shown in the experiments in section 5.2 and 5.3. Full-waveform inversion in a complex medium should include many frequency components in the inversion process in order to recover as many wavenumbers as possible.

5.6 Influence of the starting frequency

Full-waveform inversion searches for a velocity model that best explains the observed data. In other words, when forward modelling in the recovered velocity model, the residuals between the calculated data and the observed data should be as small as possible. Full-waveform inversion uses local information (the gradient) about the cost function (the ℓ^2-norm of the data residuals, eq. (2.5)) to find the direction (i.e. which model perturbations) that causes the data residuals to minimise. The waveform inverse problem is a highly non-linear problem (Sirgue, 2003), which means that the multi-dimensional cost function can be a very complex function containing several extrema. Thus the starting model should be in the neighbourhood of the global minimum, such that the gradient leads the way to the global minimum, and not a local minimum. The more linear the problem is, the greater are the chances of convergence to the global minimum. The non-linearity of the problem is dependent from both the medium itself, and some of the inversion parameters, such as frequency and maximum offset range.

In this section, simple tests for estimating the non-linearity of the problem related to frequency and offset ranges are performed. The effect considering different starting frequencies for the full-waveform inversion is also explored.

5.6.1 Description of the tests

Six different velocity models were created by smoothing the true model. These different models represent a very small selection of the total model

[5]The Marmousi model is a synthetic, heterogeneous and realistic velocity model often used as a test medium. The model is however not as complex as the 2004 BP model.

space, i.e. the number of all possible models that can explain the data. Evaluating the data residuals from this selection, can give a prediction on the behaviour of the cost function. The smoothing was applied to the true model with the *smooth2*-program (as for the starting model in section 5.2.1). The smoothing factors, in both horizontal and vertical direction, were 10, 25, 35, 50, 60 and 75. The true model, of course, corresponds to a smoothing factor of 0.

Data residuals are computed in all six models. The cost function values are then plotted with respect to the increasing smoothing factor. The cost function is normalised to the value from the last model, which in theory should represent the "worst" model. If the relationship between the perturbation of the data and the perturbation of the model are linear, the normalised cost function plot should increase linearly from 0 to 1 when going from the 1st (true model) to the last model (with smoothing factor 75). If not, the relationship is non-linear, implying that the FWI problem is non-linear and the cost function possibly has some local minima. The simple plot must not be seen as a complete description of the cost function behaviour, but an extremum in the plot strongly predicts the possibility of local minima in the cost function (Sirgue, 2003).

5.6.2 Non-linearity with respect to inverted frequencies

As mentioned in previous parts of this report (e.g. section 4.3.2), the low frequencies are more linear than the higher frequencies. In figure 5.18, the cost functions were computed in the six mentioned models for frequencies of 1, 1.5, 2, 3 and 5 Hz.

From this plot, it is evident that the full-waveform inversion in this medium is a non-linear problem. It is also clear that the non-linearity increases considerably with frequencies.

All of the frequencies in figure 5.18 have one or more maxima/minima, except at 1Hz. The first extremum appears at progressively less smoothed models for increasing frequencies. This implies that higher frequencies are more non-linear than low frequencies. As stated in the literature (e.g (Pratt et al., 1996) and (Ravaut et al., 2004)), this means that the inversion should be started at a frequency as low as possible to minimise the non-linearity of the problem. Higher starting frequencies would require better starting models to avoid converging towards a local minimum.

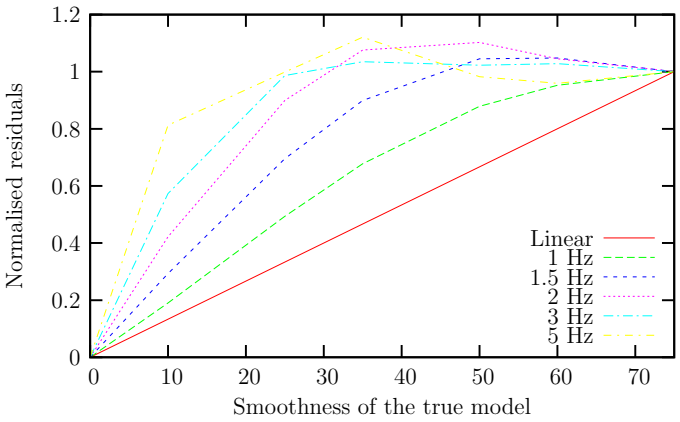

Figure 5.18: Non-linearity plot from different frequencies as a function of the smoothness of the true model

5.6.3 Starting the inversion at a higher frequency

The upper velocity model on figure 5.19 presents the result of full-waveform inversion using a starting frequency of 1.5 Hz. The starting model is the true model smoothed with a smoothing factor of 75. The regularisation parameters are

- λ=0.0001
- α=3 %
- $\vec{C}_m$: Not used

The inversion parameters and starting model are hence the same as in section 5.2, the only difference is the 1.5 Hz starting frequency. This is a very small increase of frequency, but as found in section 5.6.2, the problem will be more non-linear.

The velocity models of figure 5.19 are recovered after the inversion of the 7 Hz frequency component. The first model is the result of the inversion starting at 1.5 Hz, and the second velocity model is the successful inversion from section 5.2 starting at 1 Hz. It is easy to see the differences between these two velocity models, and it is fair to say that the full-waveform inversion for the 1.5 Hz starting frequency failed to provide a correct estimation of the velocities for most parts of the model.

Analysing velocity profiles

Velocity profiles are extracted from the two models on figure 5.19 for better comparison (see figure 5.20). From the 4005 and 7995 m velocity profiles

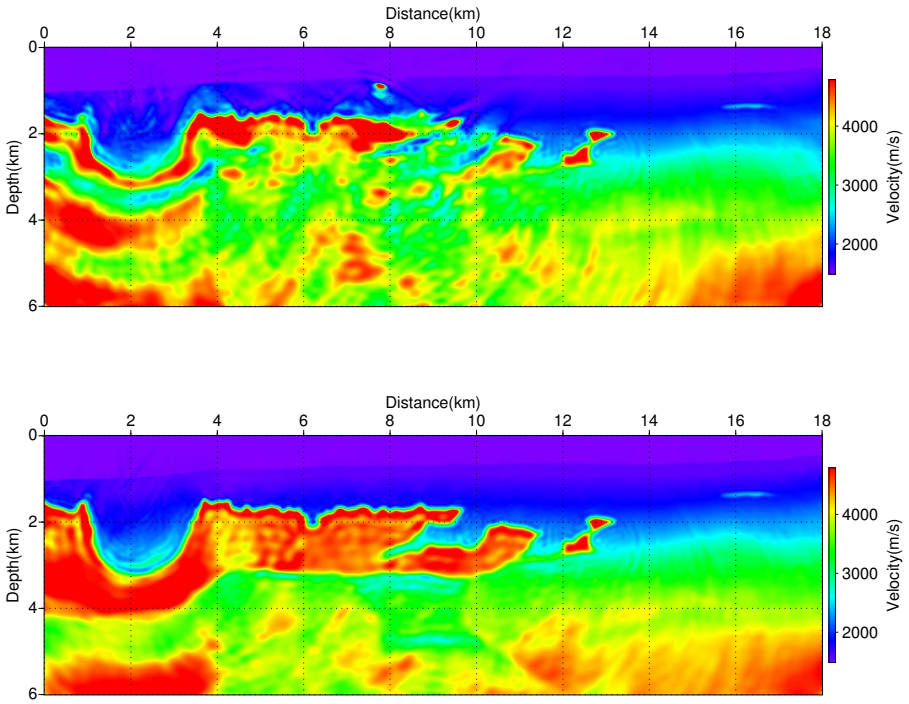

Figure 5.19: Models recovered at 7 Hz, but with different starting frequency. **Top:** Starting frequency 1.5 Hz **Bottom:** Starting frequency 1 Hz

it can be seen that the model recovered with a 1.5 Hz starting frequency have overestimated the velocities at an area between 1-1.5 km depths with approximately 500 m/s. The transition to the salt at around 1.7 km depth is recovered nicely in both profiles, but the rest of the velocities in the model starting from 1.5 Hz, are generally too oscillating and do not follow the true velocity profile nearly as good as the model recovered with a starting frequency of 1 Hz. The 13005 m velocity profile proves that the velocities are well recovered at this distance down to around 4.5 km depth.

The overall average velocity difference between the 1.5 Hz starting frequency model and the true model is more than 600 m/s for both the two first velocity profiles, while the average velocity difference is only around 250 m/s for the model starting from 1 Hz. It is therefore clear that FWI in this complex case, is very sensitive to the initial frequency due to the increase of non-linearity of the inverse problem with frequency.

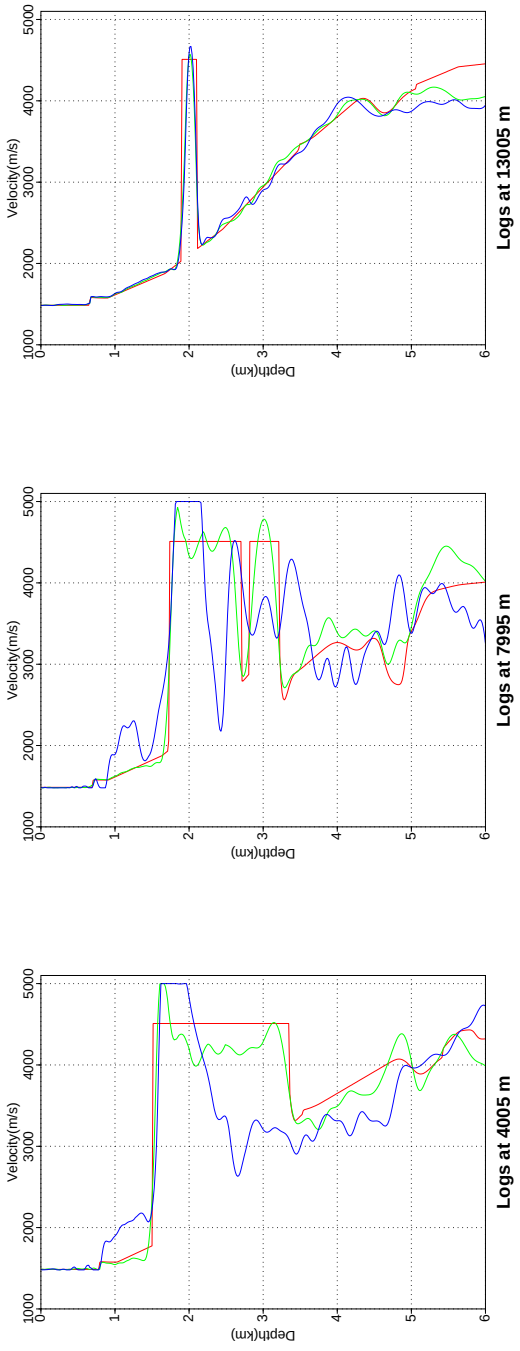

Figure 5.20: Velocity profiles extracted at 4005 m, 7995 m and 13005 m from models recovered at 7 Hz, but with the inversion started at different frequencies. Red=True model Green=1 Hz starting frequency Blue=1.5 Hz starting frequency

Data fit in the frequency domain

Even though the recovered velocity model with a 1.5 Hz starting frequency is far from the true model, the data fit between the observed and calculated data have improved. As mentioned, FWI is a method that seeks a model that best explain the observed data. The fact that the data residuals have decreased, whereas the final velocity model is not like the true one, implies that the inversion might have converged towards a local minimum of the cost function. An example of the iteratively improving data fit is presented on figure 5.21. This is an outtake of the data representing the 1st iteration at 7 Hz (green) and the 10th iteration at 7 Hz (blue), together with the observed data (red). The data represents the recordings of the last 100 receivers (located at 9-18 km) from the source fired at 375 m (shot no. 5). From this figure it is clear that both the real value and the imaginary value of the inverted data better fit the observed data after the inversion process.

The reduction of the normalised cost function value with respect to iteration number (figure 5.22), is another way to see that the data fit of the reconstructed model has improved. At each frequency, the cost function is reduced. The reduction is however significantly less than for the successful inversion with a 1 Hz starting frequency in section 5.2 (see figure 5.3). The largest, relative reduction is approximately 50 % of the initial value, and occurs for inversion of the 5 Hz frequency. In figure 5.3, the maximum reduction was approximately 90 % at 1 Hz. The small amount of reduction is another indication of convergence to a local minimum, instead of the global one.

5.6.4 Non-linearity with respect to maximum offset distance

The non-linearity of the problem might also depend from the maximum offset ranges included in the seismic data. When testing the non-linearity with respect to the offset distances, three different acquisitions with maximum offset ranges of 6, 12 and 18 km, were simulated. The source-receiver setup is outlined on figure 5.23. The data residuals were evaluated for all three acquisition types in the same six smoothed models as in section 5.6.2. Figure 5.24 shows the results for 2 Hz.

On figure 5.24, the values of the normalised data residuals of the 12 km and 18 km acquisitions are practically the same. However, the acquisition with a maximum offset distance of 6 km, express an additional extremum compared to the previous two. It is therefore likely to believe that, for this particular case, the shorter offsets might represents a more non-linear problem than longer offsets. For this reason, it is still interesting to include larger offsets in the inversion to get a better starting model and to get deeper information.

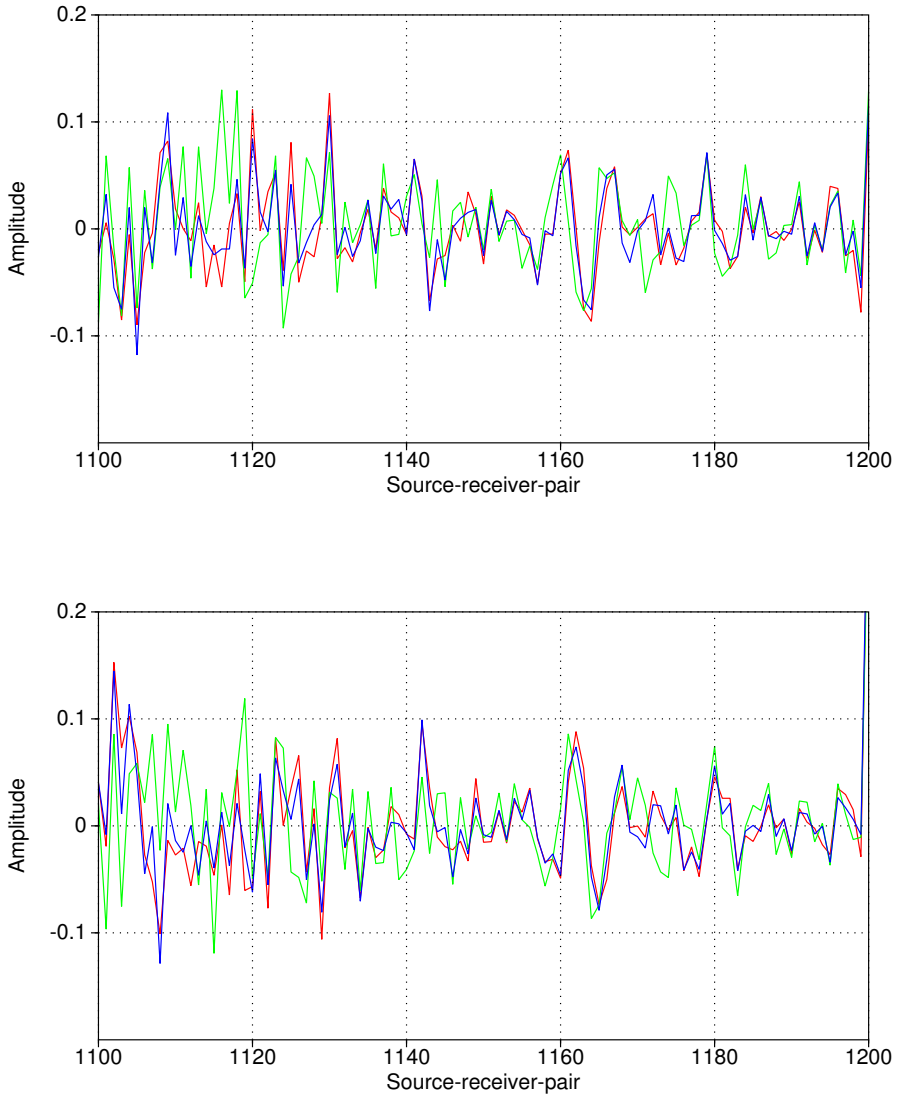

Figure 5.21: Data fit at 7 Hz for 1st and 10th iteration. Real values on top figure, imaginary values at bottom figure. The final have improved the data fit, but is not a good estimation of the true velocities. The inversion has converged to a local minimum. Red=Observed data Green=Data fit at the 1st iteration Blue=Data fit at the 10th iteration

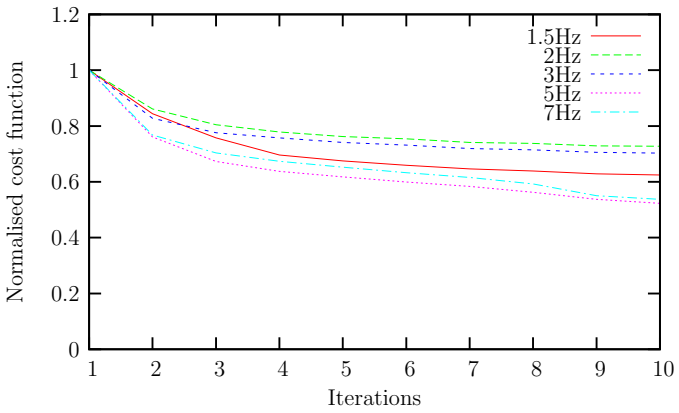

Figure 5.22: Normalised cost function with respect to iteration number for some of the frequencies in the inversion

5.7 Higher initial frequencies, better initial models

Convergence to a local minimum was somewhat expected in section 5.6, as figure 5.18 predicts local minima at 1.5 Hz for models so "far" from the global minimum as the model of smoothing factor 75. (NB! Such non-linearity curves are only possible to produce for a synthetic test where the true model is known). In the same section, it was also stated that if the starting frequency were to increase, a successful full-waveform inversion would require a better starting model. In this section FWI is conducted as in section 5.6.3, with a starting frequency of 1.5 Hz, but with an improved starting model.

The starting model

The new starting model is the true model smoothed with a smoothing factor of 35. Relying on figure 5.18, the problem should now be sufficiently linear so that the inversion might converge to the global minimum. The new starting model is the upper model presented on figure 5.25.

Parameter description

Because the inversion should be comparable to the inversion in section 5.6.3, the inversion parameters are the same:

- λ=0.0001
- α=3 %

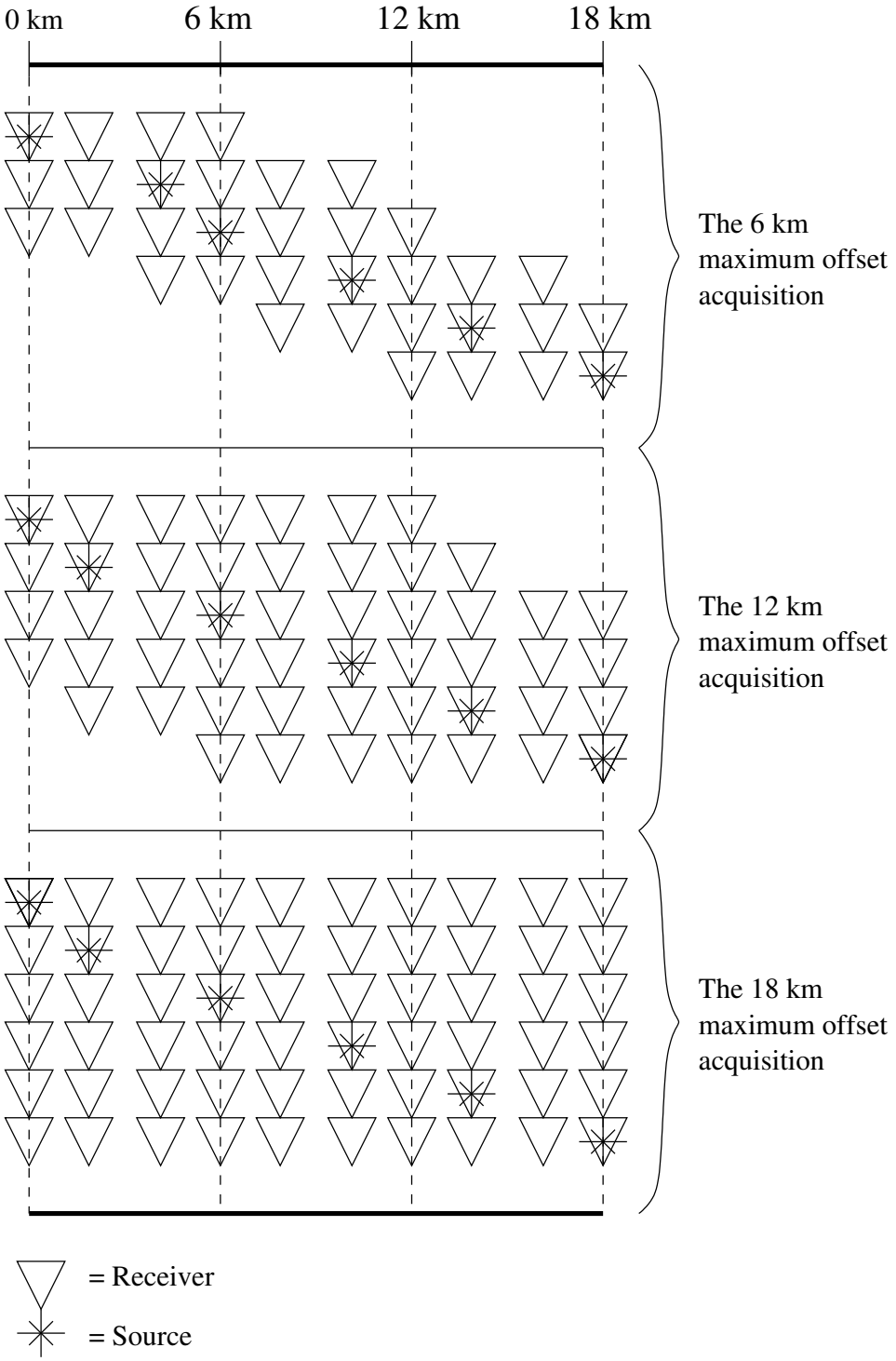

Figure 5.23: Simple figure for visualising the three acquisitions. Six sources covering the 18 km long model are shown, together with the outlay of the corresponding receiver arrays. The real acquisitions had 200 sources covering the model surface, evenly distributed 90 m apart. The corresponding receivers were also spaced every 90 m, with a maximum source-receiver distance of 6, 12 and 18 km respectively

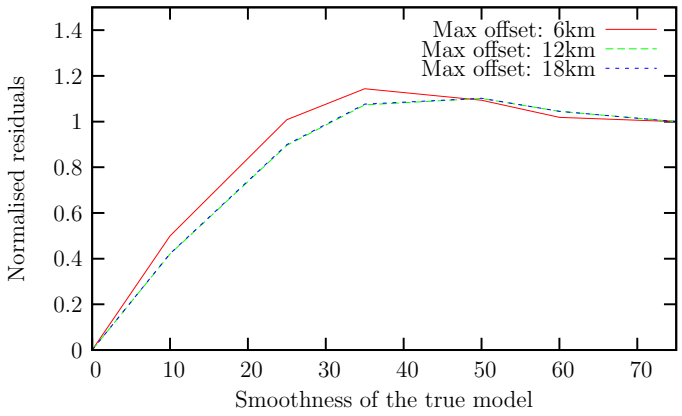

Figure 5.24: Non-linearity plot with 3 different maximum offset ranges. The frequency is 2 Hz.

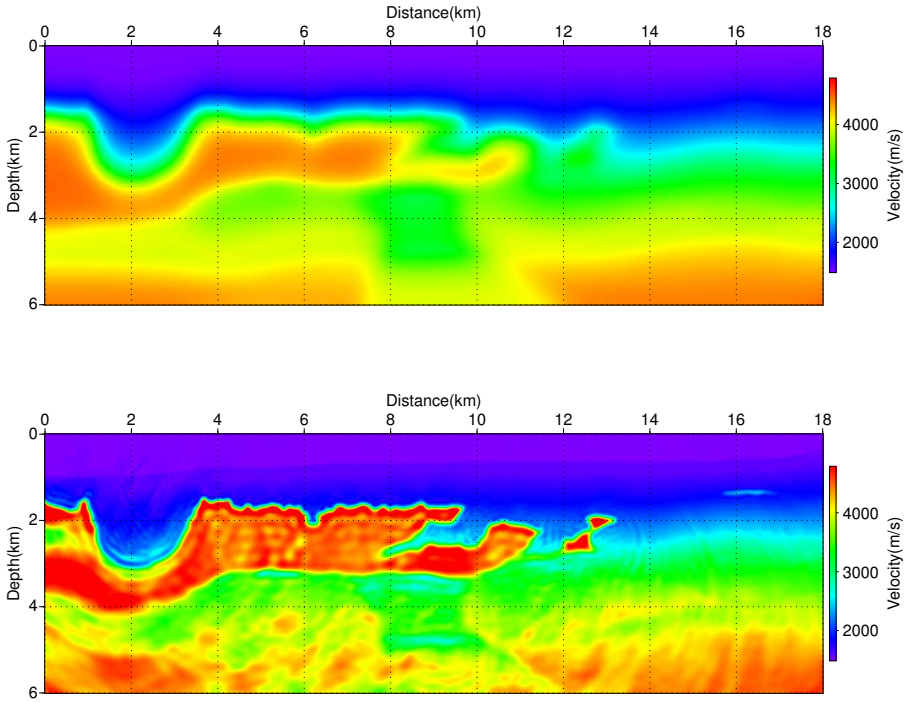

Figure 5.25: Starting model and recovered model at 7 Hz with a starting frequency of 1.5 Hz. The starting model is smoothed with a factor of 35, compared to 75 as for the models in figure 5.19

- $\vec{C}_m$: Not used

Derived velocity model

The reconstructed velocity model after the inversion of the 7 Hz frequency component is presented as the lower model in figure 5.25. The velocity model seems to estimate the salt velocities and salt boundaries just as well as the successful inversion result in section 5.2. The sub-salt velocities are also recovered to a satisfying degree. The inversion seems to have converged to the correct minimum.

Analysing velocity profiles

Figure 5.26 is a comparison between the velocity profiles from the failing inversion of section 5.6.3 (left part of the figure) and the model successfully recovered in this section (right part of the figure). The velocity profiles of both figures are recovered at 7 Hz and shown together with the velocity profile of their corresponding starting model and true model. The velocity profiles of the starting model in the left part of figure 5.26 is clearly further from the true velocity profile than the starting model in the right part of figure 5.26. This difference is enough so that the first inversion fails and the second inversion succeeds.

Commenting on the results

In the theory (chapter 4), the requirements for the starting model was assumed to be a model that could produce data residuals (in the time domain) within less than half a period of the given frequency. For a starting frequency of 1.5 Hz, the residual should therefore be less than 0.334 s ($T_{\text{residual}} < \frac{1}{2}T = \frac{1}{2f} = \frac{1}{2\times 1.5\text{s}^{-1}} \approx 0.334\text{s}$). The first-arrival traveltimes for the two starting models compared in this section (smoothed true model with smoothing factors of 75 and 35 respectively), are computed and presented in figure 5.27. Both models have first-arrival traveltime residuals higher than the estimated requirements, with absolute values of 0.60 s and 0.42 s for the 75 and 35 models respectively. However, the successful starting model had more than 98 % of the residuals within the theoretical limit, compared to 90 % that of the starting model with smoothing factor 75. When evaluating the starting model all arrivals should be compared, but it is easy to illustrate the requirements with only the first-arrivals present. The first-arrival residuals might also provide an indication on how the complete time domain data fits.

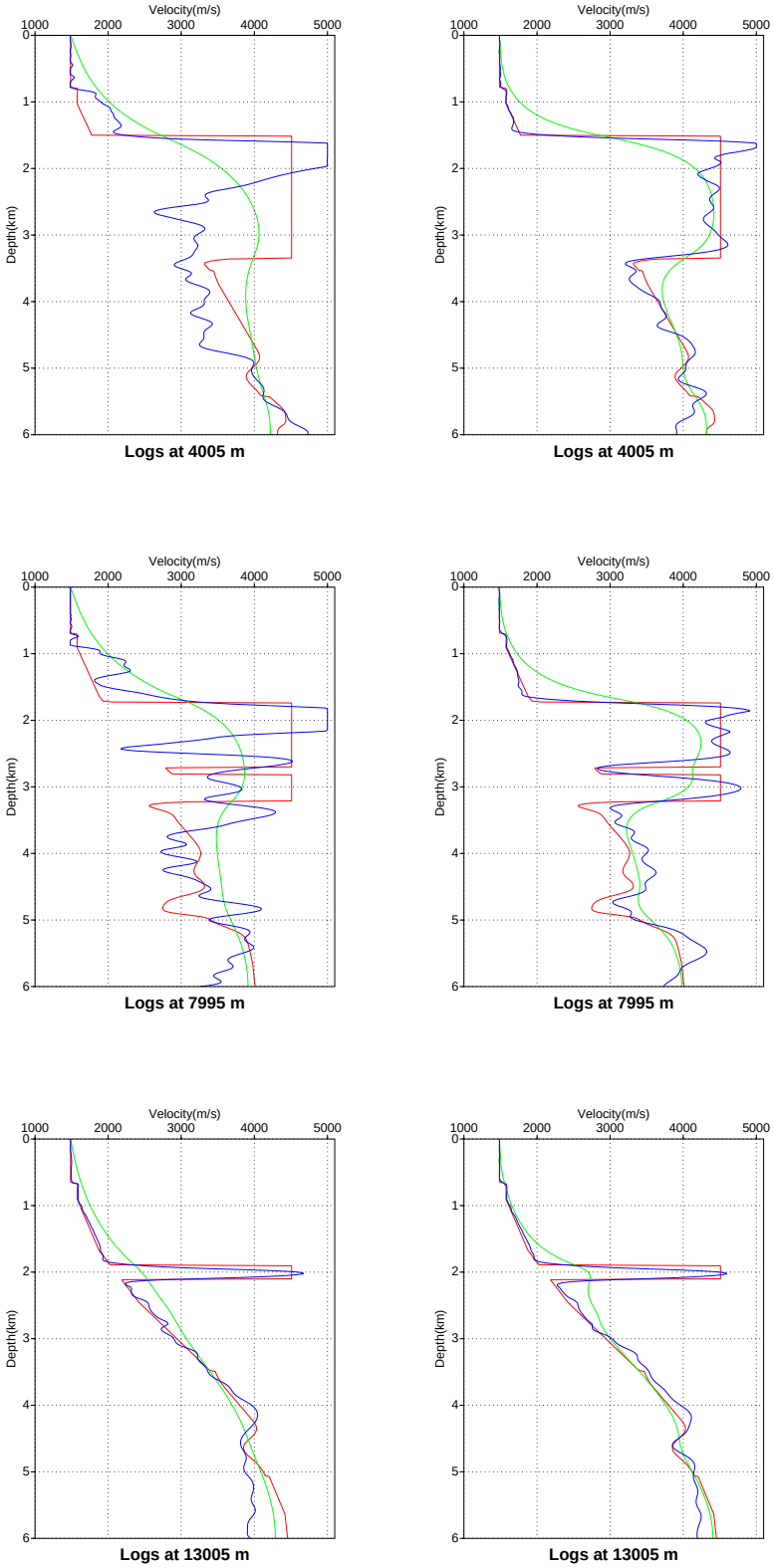

Figure 5.26: Velocity profiles extracted at 4005, 7995 and 13005 m for full-waveform inversion with a starting frequency of 1.5 Hz. **Left:** Initial model smoothed with factor 75. **Right:** Initial model smoothed with factor 35. Red=True model Green=Initial model Blue=Final model after 7 Hz

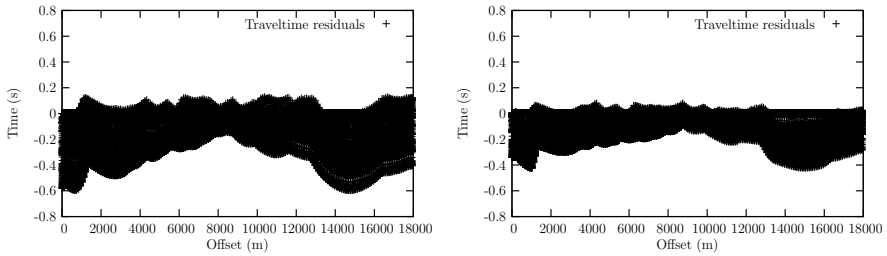

(a) Starting model with a smoothing factor of 75

(b) Starting model with a smoothing factor of 35

Figure 5.27: First-arrival traveltime residuals calculated in the two starting models with smoothing factor of 75 and 35

5.8 Conclusions

The problem presented in this thesis is more complex than many other media where the full-waveform inversion previously have been applied (e.g. simple 2-D heterogeneous models as in (Sun and McMechan, 1992), the Marmousi model as in (Sirgue and Pratt, 2004), and crustal models as in (Brenders and Pratt, 2007)). The 2004 BP benchmark velocity model contains a large salt body, and the main challenges for the velocity model estimation are the recovery of a precise delineation of the salt and a good estimation of the sub-salt velocities.

With a starting model containing the large scale features of the true model (a smoothed version of the true model), the inversion results were very good. In the recovered velocity model are the boundaries of the salt defined, and the sub-salt velocities are recovered with a deviation of as little as approximately 6 % from the true model.

A more realistic inversion was conducted using a starting model recovered from first-arrival traveltime tomography. The final estimated sub-salt velocities were more inaccurate than for the previous inversion (the sub-salt velocity deviation was approximately 10 %) because the starting model was much further from the true velocities in these deep parts of the model. However the reconstructed velocity model by FWI had improved from the starting model in all parts, and the full-waveform inversion must also in this case be called a success. Improvement of the final result could have been obtained by increasing the effort of deriving the starting model by first-arrival traveltime tomography, but this was not the main purpose of this work.

The low wavenumbers are important to recover the true velocity perturba-

tions, while the higher wavenumbers recover the shorter wavelenghts. In this complex medium, many of the wavenumbers are recovered by the frequencies used in the inversion. It is therefore important to include a sufficient amount of frequencies in the inversion process. When applying "efficient" FWI, the inversion was not able to recover as many wavenumber as the more comprehensive inversion process in section 5.2. There are, at the moment, no defined strategies for the frequency selection that will work properly in such a complex medium as the 2004 BP velocity benchmark. The recommendations based on this paper are therefore to be quite careful, and invert for a large number of low frequencies.

The non-linearity of the FWI problem increases with increasing frequencies. The more non-linear the problem is, the higher are the chances of convergence towards a local minimum, and not the global minimum of the true velocity model. The starting frequency of the inversion should therefore be kept as low as possible in order to mitigate some of the non-linearity. The higher the first inversion frequency, the higher are the requirements about the starting model.

In the very complex geological setting of the 2004 BP velocity benchmark has proven to be a very powerful tool, capable of recovering sub-salt velocities if the parameters (initial frequency, initial velocity model, offset ranges, etc.) are tuned correctly. Sub-salt imaging is still a difficult problem, but as seen in this master thesis, FWI can be a good alternative for retrieving information from such complex parts.

Chapter 6

Conclusions

6.1 Conclusions

The full-waveform inversion method and its capabilities when applied to a complex geological structure containing a salt body have been presented in this master thesis.

The FWI code used in the thesis, performs an iterative search for a velocity model that minimises the residuals between the data computed in the velocity model and the observed data, i.e. the final result is a "best fit" model. The whole wavefield, including both waveform and phase, is being used as data. All the FWI computations are implemented in the frequency domain. This ensures, amongst other things, reduction of computational cost.

The full-waveform inversion was applied to a very complex sub-part of the 2004 BP benchmark velocity model, of 18 km long by 6 km deep. The inversion result when using a smoothed version of the true velocity model as a starting model is very satisfying. 17 discrete frequencies ranging from 1 to 15 Hz were progressively included in this inversion. The large, complex salt structure is precisely delineated, for both the shallow and deeper parts. The very interesting sub-salt velocities are estimated with an approximate deviation of only 6 % from the true velocities. Low velocity anomalies below the salt were also recovered by the full-waveform inversion.

Using a starting model for the FWI derived from first-arrival traveltime tomography also provides a quite positive result. This recovered velocity model is very similar to the result using a smoothed starting model down to about 3.5 km, i.e. for velocities above and in the salt body. For the sub-salt velocities, this latter model is slightly more inaccurate, but the averaged deviation from the true velocities is still only around 10 %. The low velocity anomalies are also recovered in this velocity model. The starting model

derived from first-arrival traveltime tomography is considerably further from the true model than the smoothed starting model, in these lower parts of the medium.

The SINTEF code and some theory about first-arrival traveltime tomography were also described in the master thesis. First-arrival traveltime tomography is an efficient and stable method for deriving velocity models, even in rather complex media, but the resolution is limited to the width of the first Fresnel zone and to the recovery of the long wavelengths of the medium only. However, the final model when the method was applied to the sub-part of the 2004 BP benchmark model, is found sufficient to be used as a starting model for FWI.

Other tests were made to investigate the limits of full-waveform inversion. An inversion process using only six carefully selected frequencies (compared to seventeen frequencies in the first two applications), did not provide a satisfactory velocity model. This reconstructed model has clearly not recovered a sufficient amount of wavenumbers. To ensure good results in such a complex medium, wavenumbers must be added by including enough frequency components in the inversion process.

When using a higher starting frequency for the inversion, the recovered velocity model is far from the true model. A small test showed that lower frequencies are more linear than higher frequencies. If the starting frequency is increased, the accuracy of the starting model must therefore also be increased. Datasets including larger offset ranges were also found to increase the linearity of this particular problem.

In this master thesis, detailed and accurate velocity models were derived by full-waveform inversion in a very complex medium. The sub-salt velocities were estimated properly, where other more classical methods fail. Thus, FWI have been proven as a very interesting method for complex, sub-salt imaging. The method is very sensitive to the non-linearity of the problem, and good input parameters, such as an accurate starting model and an initial frequency as low as possible, is important for obtaining good results. Inverting a sufficient number of frequency components is also necessary for a good recovery of the wavenumber spectrum. In this work it is shown that full-waveform inversion has a great potential for estimating complex velocity models and sub-salt velocities when the acquisition parameters are as optimal as possible.

6.2 Future work

Sub-salt imaging is a difficult challenge, and research is focusing quite a lot on the topic. For future testing of FWI in such complex media, the question of starting model should be better addressed. More effort can be spent on finding a good starting model using first-arrival traveltime, stereotomography, or even a combination of the two techniques.

Applying the method to a real dataset from a geological setting similar to the synthetic BP model, would be very interesting.

The "final step" in adding the shortest wavelengths to the recovered velocity model with pre-stack depth migration was not performed in this master thesis. The impact FWI will have on the migrated image would be very important to analyse, to investigate the capabilities of FWI to improve the imaging problem in such complex media.

The FWI code should be expanded to include 3-D visco-elastic wave propagation and inversion. The inversion might also be performed by a global method, making FWI less prone to non-linearity, and reduce the requirements of the starting model. Such possible adjustments lay a bit further into the future, as they will demand, among other things, increased computational power.

If studies on sub-salt imaging, that are going in another directions than FWI (e.g. gravity, EM methods), succeed, it would be interesting to see if these could be combined with FWI, hence using all possible sources of information to reveal the sub-salt secrets.

Bibliography

Billette, F., and Brandsberg-Dahl, S., 2005, The 2004 BP Velocity Benchmark (B035), EAGE: 67th Annual Conference.

Bouchon, M., and Aki, K., 1977, Discrete wave-number representation of seismic-source wave fields: Bulletin of the Seismological Society of America, **67**, no. 2, 259–277.

Brenders, A., and Pratt, R., 2007, Full waveform tomography for lithospheric imaging: results from a blind test in a realistic crustal model: Geophysical Journal International, **168**, no. 1, 133–151.

Causse, E., 1998, Seismic migration and inversion in viso-acoustic media: Thèse, NTNU.

Chabert, A., 2007, Seismic imaging of the sedimentary and crustal structure of the hatton basin on the irish atlantic margin: Thèse, University College Dublin.

Collins, M. D., and Kuperman, W. A., 1992, Nonlinear inversion for ocean-bottom properties: The Journal of the Acoustical Society of America, , no. 92, 2770–2782.

Etgen, J. T., oct 2004, The Four Big Challenges of Subsalt Imaging, AAPG International Conference.

Fuchs, K., and Müller, G., 1971, Computation of synthetic seismograms with the reflectivity method and comparison with observations: Geophysical Journal International, **23**, no. 4, 417–433.

Gerstoft, P., 1993, Inversion of seismoacoustic data using genetic algorithms and a posteriori probability distributions: The Journal of the Acoustical Society of America, , no. 95, 770–782.

Hovem, J. M., 2007, Marin Acoustics - The Physics of Sound in Underwater Environments: Not yet published.

Improta, L., Zollo, A., Herrero, A., Frattini, R., Virieux, J., and Dell'Aversana, P., 2002, Seismic imaging of complex structures by non-

linear traveltime inversion of dense wide-angle data: application to a thrust belt: Geophysical Journal International, **151**, no. 1, 264–278.

Kinsler, L., Frey, A., Coppens, A., and Sanders, J., 2000, Fundamentals of Acoustics: John Wiley & Sons, Inc., 4 edition.

Mora, P., 1987, Elastic wavefield inversion: Thèse, Stanford University.

Operto, S., Ravaut, C., Improta, L., Virieux, J., Herrero, A., and Dell'Aversana, P., 2004, Quantitative imaging of complex structures from dense wide-aperture seismic data by multiscale traveltime and waveform inversions: a case study: Geophysical Prospecting, **52**, no. 6, 625–651.

Paige, C. C., and Saunders, M. A., 1982, LSQR: An algorithm for sparse linear equations and sparse least squares: ACM Transactions on Mathematical Software, **8**, no. 1, 43–71.

Podvin, P., and Lecomte, I., 1991, Finite difference computation of traveltimes in very contrasted velocity models: a massively parallel approach and its associated tools: Geophysical Journal International, **105**, no. 1, 271–284.

Pratt, R., and Worthington, M., 1990, Inverse theory applied to multi-source cross-hole tomography. part 1: Acoustic wave-equation method: Geophysical Prospecting, **38**, no. 3, 287–301.

Pratt, R., Song, Z.-M., Williamson, P., and Warner, M., 1996, Two-dimentional velocity models from wide-angle seismic data by wavefield inversion: Geophysical Journal International, **124**, no. 2, 323–340.

Pratt, R., Shin, C., and Hicks, G., 1998, Gauss-newton and full newton methods in frequency-space seismic waveform inversion: Geophysical Journal International, **133**, no. 2, 341–362.

Ravaut, C., Operto, S., Improta, L., Virieux, J., Herrero, A., and Dell'Aversana, P., 2004, Multiscale imaging of complex structures from multifold wide-aperture seismic data by frequency-domain full-waveform tomography: application to a thrust belt: Geophysical Journal International, **159**, no. 3, 1032–1056.

Ravaut, C., 2003, Tomographie sismique haute resolution de la croute terrestre :inversion combinee des temps de trajets et des formes d'ondes de donneesde sismique refraction/reflexion grand-angle mutitrace: Thèse, Université Paris VI.

Singer, P., 2005, Subsalt Imaging: Is the Salt Winning?: Subsalt Imaging: Is the Salt Winning?:, Center for Wave Phenomena, Colorado School of Mines, Workshop on Subsalt Imaging Problems: Practical Problems Seeking Solutions.

Sirgue, L., and Pratt, R., 2004, Efficient waveform inversion and imaging: A strategy for selecting temporal frequencies: Geophysics, **69**, no. 1, 231–248.

Sirgue, L., 2003, Frequency domain waveform inversion of large offset seismic data: Thèse, l'Ecole Normale Superieure de Paris.

Sun, R., and McMechan, G. A., 1992, 2-D full-wavefield inversion for wide-aperture, elastic, seismic data: Geophysical Journal International, **111**, no. 1, 1–10.

Tarantola, A., 1986, A strategy for nonlinear elastic inversion of seismic reflection data: Geophysics, **51**, no. 10, 1893–1903.

Thomassen, E., Dec 2007, 2D Velocity estimation by stereotomography for salt imaging, Department of Electronics and Telecommunications, NTNU, Project work in the course TTT4550.

Červený, V., Molotkov, I., and Pšenšik, I., 1977, Ray method in seismology: University of Karlova, Prague, Czechoslovakia.

Štekl, I., 1997, Frequency domain seismic forward modelling: A tool for waveform inversion: Thèse, Imperial College London.

Appendix A

Programs used in the master thesis

A list of programs used in this master thesis, and a short description on how they are used:

- The FWI program - *For running the full-waveform inversion. A SINTEF code*
- The first-arrival traveltime tomography program - *For running the first-arrival traveltime tomography. A SINTEF code*
- A ray tracing program - *For running raytracing in a velocity model. A SINTEF code*
- refractedRayfix.m - *A code for changing the reflected ray tracing file from the raytracing program so that the reflection angle and slope of the reflection point can be altered. Code in A.1*
- vLogLayerStat.m - *A code for deriving statistics from the velocity profiles (as in figure 5.17). Code in A.2*
- ttresiduals.m - *A code for obtaining the first-arrival traveltime residuals with respect to the offset distance. Code in A.3*
- createVM.m - *A code for creating 1-D (gradient) velocity models. Code in A.4*

All codes shown in this appendix are written in MATLAB (not the SINTEF codes). The script are written as small helpers in order to retreive wanted information etc. Optimalisation of the code, and a language readable to others was not prioritised in the making.

A.1 reflectedRayFix.m

```
%%%%%%%%%%%%%%%%%%%%%%%%%%%%%%%%%%%%%%%%%%%%
%Written by Espen Thomassen, spring 2008.
%Script for changing the mouse-click-diffraction/reflection-points-file to a fil
%%%%%%%%%%%%%%%%%%%%%%%%%%%%%%%%%%%%%%%%%%%%

%load mouse-click file (reflection points):
points=load('diffpoints.txt');

%Set the variables (angle of rays leaving the reflection point)
%angleA=-2.54159;
%angleB= 2.54159;
%angleA=-2.3562; %45 deg (really 135 deg)
%angleB= 2.3562; %45 deg
angleA=-2.65; %ca. 30 deg (really 150 deg)
angleB= 2.65; %ca. 30 deg
formA=3;
formB=3;


%help matrix
pointsTMP=points;


%%%%%%%%%%%%%%%%%%%%%%%%%%%%%
%dip test part 1
for i=1:(length(points(:,1))-1);

theta1(i)=(points(i,1)-points((i+1),1))/(points(i,2)-points((i+1),2));
theta2(i)=abs(theta1(i));
theta3(i)=atan(theta2(i));

if theta3(i)>0.45

if points(i,1)>points((i+1),1) && points(i,2)<points((i+1),2)
angle1(i)=theta3(i)+angleA;
angle2(i)=theta3(i)+angleB;

elseif points(i,1)<points((i+1),1) && points(i,2)<points((i+1),2)
angle1(i)=theta3(i)+angleA+(3*pi/2);
angle2(i)=theta3(i)+angleB+(3*pi/2);
```

```
elseif points(i,1)<points((i+1),1) && points(i,2)>points((i+1),2)
angle1(i)=theta3(i)+angleA-(pi);
angle2(i)=theta3(i)+angleB-(pi);

else %points(i,1)<points((i+1),1) && points(i,2)>points((i+1),2)
angle1(i)=theta3(i)+angleA+(pi/2);
angle2(i)=theta3(i)+angleB+(pi/2);
end

else
 angle1(i)=theta3(i)+angleA;
angle2(i)=theta3(i)+angleB;
end
end

%%%%%%%%%%%%%%%%%%%%%%%%%%%%


%Swapping the coloums
points(:,1)=pointsTMP(:,2)./1000;
points(:,2)=pointsTMP(:,1)./1000;

%%%%%%%%%%%%%%%%%%%%%%%%%%%%%%%%%%%%%%%%%%%%
%dip test part 2
remove=2:2:(length(points(:,1)))-1;
points(remove,:)=[];
angle1(:,remove)=[];
angle2(:,remove)=[];

points((length(points(:,1))),:)=[];
%%%%%%%%%%%%%%%%%%%%%%%%%%%%%%%%%%%%%%%%%%%%

%Add coloums with information about 2xAngles and type of wave
points(:,3)=angle1;
points(:,4)=angle2;
points(:,5)=formA;
points(:,6)=formB;

%save as a new file in ascii format
save diffpointsFixed.txt points -ascii;
disp('Ray file created')
%EOF
```

A.2 vLogLayerStat.m

```
%%%%%%%%%%%%%%%%%%%%%%%%%%%%%%%%%%%%%%%%%%%%
%Written by Espen Thomassen, spring 2008
%Calculate the avarage (rms) deviation between the true velocity profile and a v
%%%%%%%%%%%%%%%%%%%%%%%%%%%%%%%%%%%%%%%%%%%%

clear;

%Choose log-number:
log=867;
logstring=num2str(log);

%Choose frequency:
freq=7;
freqstring=num2str(freq);

%Load models. Needs to be ascii format:
name1=['true-log',logstring,'.a'];
name2=['fixed-',freqstring,'Hz-it10-log',logstring,'.a'];
true=load(name1);
model1=load(name2);

%%%%%%%%%%%%%%%%%%%%%%%%%%%%%%%%%%%%%%%%%%%%
%Creating one long vector of the models:
b=true(1,:);
c=model1(1,:);
for i=2:200;
    a=true(i,:);
    b=[b a];
    truelang=transpose(b);

    d=model1(i,:);
    c=[c d];
    model1lang=transpose(c);
end

%Velocity difference for the entire model:
diff=truelang-model1lang;
diffabs=abs(diff);
sqdiff=diff.^2;
sumsqdiff=sum(sum(sqdiff));
meansumsqdiff=sumsqdiff/400;
```

```
rootmeansumsqdiff=sqrt(meansumsqdiff);
[Y,I]=max(diffabs);
prodiff=(Y/truelang(I))*100;



%%%%%%%%%%%%%%%%%%%%%%%%%%%%%%%%%%%%%%%%%%%%%%%%%%%%%%%%%%%%%%%%%%%%%%%
%Compute velocity difference for profile divided in 3 zones:
%The zones are found manually for each of the pre defined profiles.

%Velocity profile at nx=53 (equals 795 m):
if log==53;
zone1log53=1:105;
zone2log53=106:276;
zone3log53=277:400;
truez1=truelang(zone1log53);
modelz1=model1lang(zone1log53);
truez2=truelang(zone2log53);
modelz2=model1lang(zone2log53);
truez3=truelang(zone3log53);
modelz3=model1lang(zone3log53);

diffz1=truez1-modelz1;
diffabsz1=abs(diffz1);
sqdiffz1=diffz1.^2;
sumsqdiffz1=sum(sum(sqdiffz1));
meansumsqdiffz1=sumsqdiffz1/length(truez1);
rootmeansumsqdiffz1=sqrt(meansumsqdiffz1);
[Yz1,Iz1]=max(diffabsz1);
prodiffz1=(Yz1/truez1(Iz1))*100;
mvz1=mean(truez1);
prodiffrmsz1=(rootmeansumsqdiffz1/mvz1)*100;

diffz2=truez2-modelz2;
diffabsz2=abs(diffz2);
sqdiffz2=diffz2.^2;
sumsqdiffz2=sum(sum(sqdiffz2));
meansumsqdiffz2=sumsqdiffz2/length(truez2);
rootmeansumsqdiffz2=sqrt(meansumsqdiffz2);
[Yz2,Iz2]=max(diffabsz2);
prodiffz2=(Yz2/truez2(Iz2))*100;
mvz2=mean(truez2);
prodiffrmsz2=(rootmeansumsqdiffz2/mvz2)*100;
```

```
diffz3=truez3-modelz3;
diffabsz3=abs(diffz3);
sqdiffz3=diffz3.^2;
sumsqdiffz3=sum(sum(sqdiffz3));
meansumsqdiffz3=sumsqdiffz3/length(truez3);
rootmeansumsqdiffz3=sqrt(meansumsqdiffz3);
[Yz3,Iz3]=max(diffabsz3);
prodiffz3=(Yz3/truez3(Iz3))*100;
mvz3=mean(truez3);
prodiffrmsz3=(rootmeansumsqdiffz3/mvz3)*100;

%Velocity profile at nx=133:
elseif log==133;
zone1log133=1:211;
zone2log133=212:275;
zone3log133=276:400;
truez1=truelang(zone1log133);
modelz1=model1lang(zone1log133);
truez2=truelang(zone2log133);
modelz2=model1lang(zone2log133);
truez3=truelang(zone3log133);
modelz3=model1lang(zone3log133);

diffz1=truez1-modelz1;
diffabsz1=abs(diffz1);
sqdiffz1=diffz1.^2;
sumsqdiffz1=sum(sum(sqdiffz1));
meansumsqdiffz1=sumsqdiffz1/length(truez1);
rootmeansumsqdiffz1=sqrt(meansumsqdiffz1);
[Yz1,Iz1]=max(diffabsz1);
prodiffz1=(Yz1/truez1(Iz1))*100;
mvz1=mean(truez1);
prodiffrmsz1=(rootmeansumsqdiffz1/mvz1)*100;

diffz2=truez2-modelz2;
diffabsz2=abs(diffz2);
sqdiffz2=diffz2.^2;
sumsqdiffz2=sum(sum(sqdiffz2));
meansumsqdiffz2=sumsqdiffz2/length(truez2);
rootmeansumsqdiffz2=sqrt(meansumsqdiffz2);
[Yz2,Iz2]=max(diffabsz2);
prodiffz2=(Yz2/truez2(Iz2))*100;
mvz2=mean(truez2);
prodiffrmsz2=(rootmeansumsqdiffz2/mvz2)*100;
```

```
diffz3=truez3-modelz3;
diffabsz3=abs(diffz3);
sqdiffz3=diffz3.^2;
sumsqdiffz3=sum(sum(sqdiffz3));
meansumsqdiffz3=sumsqdiffz3/length(truez3);
rootmeansumsqdiffz3=sqrt(meansumsqdiffz3);
[Yz3,Iz3]=max(diffabsz3);
prodiffz3=(Yz3/truez3(Iz3))*100;
mvz3=mean(truez3);
prodiffrmsz3=(rootmeansumsqdiffz3/mvz3)*100;


%Velocity profile at nx=267:
elseif log==267;
zone1log267=1:100;
zone2log267=101:223;
zone3log267=224:400;
truez1=truelang(zone1log267);
modelz1=model1lang(zone1log267);
truez2=truelang(zone2log267);
modelz2=model1lang(zone2log267);
truez3=truelang(zone3log267);
modelz3=model1lang(zone3log267);

diffz1=truez1-modelz1;
diffabsz1=abs(diffz1);
sqdiffz1=diffz1.^2;
sumsqdiffz1=sum(sum(sqdiffz1));
meansumsqdiffz1=sumsqdiffz1/length(truez1);
rootmeansumsqdiffz1=sqrt(meansumsqdiffz1);
[Yz1,Iz1]=max(diffabsz1);
prodiffz1=(Yz1/truez1(Iz1))*100;
mvz1=mean(truez1);
prodiffrmsz1=(rootmeansumsqdiffz1/mvz1)*100;

diffz2=truez2-modelz2;
diffabsz2=abs(diffz2);
sqdiffz2=diffz2.^2;
sumsqdiffz2=sum(sum(sqdiffz2));
meansumsqdiffz2=sumsqdiffz2/length(truez2);
rootmeansumsqdiffz2=sqrt(meansumsqdiffz2);
[Yz2,Iz2]=max(diffabsz2);
prodiffz2=(Yz2/truez2(Iz2))*100;
```

```
mvz2=mean(truez2);
prodiffrmsz2=(rootmeansumsqdiffz2/mvz2)*100;

diffz3=truez3-modelz3;
diffabsz3=abs(diffz3);
sqdiffz3=diffz3.^2;
sumsqdiffz3=sum(sum(sqdiffz3));
meansumsqdiffz3=sumsqdiffz3/length(truez3);
rootmeansumsqdiffz3=sqrt(meansumsqdiffz3);
[Yz3,Iz3]=max(diffabsz3);
prodiffz3=(Yz3/truez3(Iz3))*100;
mvz3=mean(truez3);
prodiffrmsz3=(rootmeansumsqdiffz3/mvz3)*100;

%Velocity profile at nx=380:
elseif log==380;
zone1log380=1:110;
zone2log380=111:211;
zone3log380=212:400;
truez1=truelang(zone1log380);
modelz1=model1lang(zone1log380);
truez2=truelang(zone2log380);
modelz2=model1lang(zone2log380);
truez3=truelang(zone3log380);
modelz3=model1lang(zone3log380);

diffz1=truez1-modelz1;
diffabsz1=abs(diffz1);
sqdiffz1=diffz1.^2;
sumsqdiffz1=sum(sum(sqdiffz1));
meansumsqdiffz1=sumsqdiffz1/length(truez1);
rootmeansumsqdiffz1=sqrt(meansumsqdiffz1);
[Yz1,Iz1]=max(diffabsz1);
prodiffz1=(Yz1/truez1(Iz1))*100;
mvz1=mean(truez1);
prodiffrmsz1=(rootmeansumsqdiffz1/mvz1)*100;

diffz2=truez2-modelz2;
diffabsz2=abs(diffz2);
sqdiffz2=diffz2.^2;
sumsqdiffz2=sum(sum(sqdiffz2));
meansumsqdiffz2=sumsqdiffz2/length(truez2);
rootmeansumsqdiffz2=sqrt(meansumsqdiffz2);
[Yz2,Iz2]=max(diffabsz2);
```

```
prodiffz2=(Yz2/truez2(Iz2))*100;
mvz2=mean(truez2);
prodiffrmsz2=(rootmeansumsqdiffz2/mvz2)*100;

diffz3=truez3-modelz3;
diffabsz3=abs(diffz3);
sqdiffz3=diffz3.^2;
sumsqdiffz3=sum(sum(sqdiffz3));
meansumsqdiffz3=sumsqdiffz3/length(truez3);
rootmeansumsqdiffz3=sqrt(meansumsqdiffz3);
[Yz3,Iz3]=max(diffabsz3);
prodiffz3=(Yz3/truez3(Iz3))*100;
mvz3=mean(truez3);
prodiffrmsz3=(rootmeansumsqdiffz3/mvz3)*100;

%Velocity profile at nx=533:
elseif log==533;
zone1log533=1:115;
zone2log533=116:214;
zone3log533=215:400;
truez1=truelang(zone1log533);
modelz1=model1lang(zone1log533);
truez2=truelang(zone2log533);
modelz2=model1lang(zone2log533);
truez3=truelang(zone3log533);
modelz3=model1lang(zone3log533);

diffz1=truez1-modelz1;
diffabsz1=abs(diffz1);
sqdiffz1=diffz1.^2;
sumsqdiffz1=sum(sum(sqdiffz1));
meansumsqdiffz1=sumsqdiffz1/length(truez1);
rootmeansumsqdiffz1=sqrt(meansumsqdiffz1);
[Yz1,Iz1]=max(diffabsz1);
prodiffz1=(Yz1/truez1(Iz1))*100;
mvz1=mean(truez1);
prodiffrmsz1=(rootmeansumsqdiffz1/mvz1)*100;

diffz2=truez2-modelz2;
diffabsz2=abs(diffz2);
sqdiffz2=diffz2.^2;
sumsqdiffz2=sum(sum(sqdiffz2));
meansumsqdiffz2=sumsqdiffz2/length(truez2);
rootmeansumsqdiffz2=sqrt(meansumsqdiffz2);
```

```
[Yz2,Iz2]=max(diffabsz2);
prodiffz2=(Yz2/truez2(Iz2))*100;
mvz2=mean(truez2);
prodiffrmsz2=(rootmeansumsqdiffz2/mvz2)*100;

diffz3=truez3-modelz3;
diffabsz3=abs(diffz3);
sqdiffz3=diffz3.^2;
sumsqdiffz3=sum(sum(sqdiffz3));
meansumsqdiffz3=sumsqdiffz3/length(truez3);
rootmeansumsqdiffz3=sqrt(meansumsqdiffz3);
[Yz3,Iz3]=max(diffabsz3);
prodiffz3=(Yz3/truez3(Iz3))*100;
mvz3=mean(truez3);
prodiffrmsz3=(rootmeansumsqdiffz3/mvz3)*100;

%Velocity profile at nx=667:
elseif log==667;
zone1log667=1:166;
zone2log667=167:213;
zone3log667=214:400;
truez1=truelang(zone1log667);
modelz1=model1lang(zone1log667);
truez2=truelang(zone2log667);
modelz2=model1lang(zone2log667);
truez3=truelang(zone3log667);
modelz3=model1lang(zone3log667);

diffz1=truez1-modelz1;
diffabsz1=abs(diffz1);
sqdiffz1=diffz1.^2;
sumsqdiffz1=sum(sum(sqdiffz1));
meansumsqdiffz1=sumsqdiffz1/length(truez1);
rootmeansumsqdiffz1=sqrt(meansumsqdiffz1);
[Yz1,Iz1]=max(diffabsz1);
prodiffz1=(Yz1/truez1(Iz1))*100;
mvz1=mean(truez1);
prodiffrmsz1=(rootmeansumsqdiffz1/mvz1)*100;

diffz2=truez2-modelz2;
diffabsz2=abs(diffz2);
sqdiffz2=diffz2.^2;
sumsqdiffz2=sum(sum(sqdiffz2));
meansumsqdiffz2=sumsqdiffz2/length(truez2);
```

```
rootmeansumsqdiffz2=sqrt(meansumsqdiffz2);
[Yz2,Iz2]=max(diffabsz2);
prodiffz2=(Yz2/truez2(Iz2))*100;
mvz2=mean(truez2);
prodiffrmsz2=(rootmeansumsqdiffz2/mvz2)*100;

diffz3=truez3-modelz3;
diffabsz3=abs(diffz3);
sqdiffz3=diffz3.^2;
sumsqdiffz3=sum(sum(sqdiffz3));
meansumsqdiffz3=sumsqdiffz3/length(truez3);
rootmeansumsqdiffz3=sqrt(meansumsqdiffz3);
[Yz3,Iz3]=max(diffabsz3);
prodiffz3=(Yz3/truez3(Iz3))*100;
mvz3=mean(truez3);
prodiffrmsz3=(rootmeansumsqdiffz3/mvz3)*100;

%Velocity profile at nx=800:
elseif log==800;
zone1log800=1:176;
zone2log800=177:186;
zone3log800=187:400;
truez1=truelang(zone1log800);
modelz1=model1lang(zone1log800);
truez2=truelang(zone2log800);
modelz2=model1lang(zone2log800);
truez3=truelang(zone3log800);
modelz3=model1lang(zone3log800);

diffz1=truez1-modelz1;
diffabsz1=abs(diffz1);
sqdiffz1=diffz1.^2;
sumsqdiffz1=sum(sum(sqdiffz1));
meansumsqdiffz1=sumsqdiffz1/length(truez1);
rootmeansumsqdiffz1=sqrt(meansumsqdiffz1);
[Yz1,Iz1]=max(diffabsz1);
prodiffz1=(Yz1/truez1(Iz1))*100;
mvz1=mean(truez1);
prodiffrmsz1=(rootmeansumsqdiffz1/mvz1)*100;

diffz2=truez2-modelz2;
diffabsz2=abs(diffz2);
sqdiffz2=diffz2.^2;
sumsqdiffz2=sum(sum(sqdiffz2));
```

```
meansumsqdiffz2=sumsqdiffz2/length(truez2);
rootmeansumsqdiffz2=sqrt(meansumsqdiffz2);
[Yz2,Iz2]=max(diffabsz2);
prodiffz2=(Yz2/truez2(Iz2))*100;
mvz2=mean(truez2);
prodiffrmsz2=(rootmeansumsqdiffz2/mvz2)*100;

diffz3=truez3-modelz3;
diffabsz3=abs(diffz3);
sqdiffz3=diffz3.^2;
sumsqdiffz3=sum(sum(sqdiffz3));
meansumsqdiffz3=sumsqdiffz3/length(truez3);
rootmeansumsqdiffz3=sqrt(meansumsqdiffz3);
[Yz3,Iz3]=max(diffabsz3);
prodiffz3=(Yz3/truez3(Iz3))*100;
mvz3=mean(truez3);
prodiffrmsz3=(rootmeansumsqdiffz3/mvz3)*100;

%Velocity profile at nx=867:
else
zone1log867=1:126;
zone2log867=127:140;
zone3log867=141:400;
truez1=truelang(zone1log867);
modelz1=model1lang(zone1log867);
truez2=truelang(zone2log867);
modelz2=model1lang(zone2log867);
truez3=truelang(zone3log867);
modelz3=model1lang(zone3log867);

diffz1=truez1-modelz1;
diffabsz1=abs(diffz1);
sqdiffz1=diffz1.^2;
sumsqdiffz1=sum(sum(sqdiffz1));
meansumsqdiffz1=sumsqdiffz1/length(truez1);
rootmeansumsqdiffz1=sqrt(meansumsqdiffz1);
[Yz1,Iz1]=max(diffabsz1);
prodiffz1=(Yz1/truez1(Iz1))*100;
mvz1=mean(truez1);
prodiffrmsz1=(rootmeansumsqdiffz1/mvz1)*100;

diffz2=truez2-modelz2;
diffabsz2=abs(diffz2);
sqdiffz2=diffz2.^2;
```

```
sumsqdiffz2=sum(sum(sqdiffz2));
meansumsqdiffz2=sumsqdiffz2/length(truez2);
rootmeansumsqdiffz2=sqrt(meansumsqdiffz2);
[Yz2,Iz2]=max(diffabsz2);
prodiffz2=(Yz2/truez2(Iz2))*100;
mvz2=mean(truez2);
prodiffrmsz2=(rootmeansumsqdiffz2/mvz2)*100;

diffz3=truez3-modelz3;
diffabsz3=abs(diffz3);
sqdiffz3=diffz3.^2;
sumsqdiffz3=sum(sum(sqdiffz3));
meansumsqdiffz3=sumsqdiffz3/length(truez3);
rootmeansumsqdiffz3=sqrt(meansumsqdiffz3);
[Yz3,Iz3]=max(diffabsz3);
prodiffz3=(Yz3/truez3(Iz3))*100;
mvz3=mean(truez3);
prodiffrmsz3=(rootmeansumsqdiffz3/mvz3)*100;
end;


%%%%%%%%%%%%%%%%%%%%%%%%%%%%%%%%%%%%%%%%%%%%%%%%%%%%
%Display results on screen:
disp(' ')
disp(['Frequency: ',freqstring,' Log: ', logstring]);
disp('Totalt:');
disp(['Average deviation is ', num2str(rootmeansumsqdiff), 'm/s'])
disp(['The largest deviation has an absoloute value of ', num2str(Y), 'm/s,'])
disp([' this is a derviation of ',num2str(prodiff), '% from the true value.'])
disp(['mean=',num2str(mean(diff))])
disp(['std=',num2str(std(diff))])
disp(['var=',num2str(var(diff))])
disp('');
disp(['Avg dev z1: ',num2str(rootmeansumsqdiffz1), ' - ',num2str(prodiffrmsz1), '% of ',
disp(['Avg dev z2: ',num2str(rootmeansumsqdiffz2), ' - ',num2str(prodiffrmsz2), '% of ',
disp(['Avg dev z3: ',num2str(rootmeansumsqdiffz3), ' - ',num2str(prodiffrmsz3), '% of ',
disp(['Largest dev z1: ',num2str(Yz1), ' - ',num2str(prodiffz1),'%'])
disp(['Largest dev z2: ',num2str(Yz2), ' - ',num2str(prodiffz2),'%'])
disp(['Largest dev z3: ',num2str(Yz3), ' - ',num2str(prodiffz3),'%'])

%EOF
```

A.3 ttresiduals.m

```
%%%%%%%%%%%%%%%%%%%%%%%%%%%%%%%%%%%%%%%%%
%Written by Espen Thomassen, spring 2008
%Compute traveltime residuals from "facqui.out" files
%%%%%%%%%%%%%%%%%%%%%%%%%%%%%%%%%%%%%%%%%

%The facqui files must be loaded in the MATLAB workspace in advance.
%(file-->import data-->filename).

%help vector for selecting traveltimes
select=1:2:length(facqui1)-1;

%selecting offsetvalues and traveltimes
tttrue=facquitomo(select,(2:3));
tt1=facqui1(select,(2:3));
ttfinal=facqui10(select,(2:3));

%creating traveltime residuals
ttresidual1=tttrue;
ttresidualfinal=tttrue;
ttresidual1(:,2)=tttrue(:,2)-tt1(:,2);
ttresidualfinal(:,2)=tttrue(:,2)-ttfinal(:,2);

%sort by offset values (not necessary)
ttresidual1=sortrows(ttresidual1);
ttresidualfinal=sortrows(ttresidualfinal);

%save the residuals
save residual1.ascii ttresidual1 -ascii;
save residualfinal.ascii ttresidualfinal -ascii;

%EOF
```

A.4 createVM.m

```
%%%%%%%%%%%%%%%%%%%%%%%%%%%%%%%%%%%%%%%%
%Written by Espen Thomassen, spring 2008.
%Creating 1-D gradient velocity models
%%%%%%%%%%%%%%%%%%%%%%%%%%%%%%%%%%%%%%%%
```

```
%%%%%%%%%%%%%%%%%%%%%%%%%%%%%%%%%
%Defining the variables:
h=15;           %mesh spacing
nx=1201;        %horizontal nodal points
nz=401;         %vertical nodal points
vtop=1500;      %starting velocity
vgradient=0.6;  %velocity gradient

%%%%%%%%%%%%%%%%%%%%%%%%%%%%%%%%%
%helper calculations:
a1=0:(nz-1);
a2=a1*15;
a3=a2;

for i=1:(nx);
    a3=[a3 a2];
end

b1=vtop+(vgradient*a3);

left=1:2:(length(b1));
right=2:2:(length(b1));

%%%%%%%%%%%%%%%%%%%%%%%%%%%%%%%%%
%Create velocity model matrix:
vmodel=[transpose(b1(left)) transpose(b1(right))];

%%%%%%%%%%%%%%%%%%%%%%%%%%%%%%%%%
%Save velocity model in ascii format:
save vstart.ascii vmodel -ascii;
disp('Model built. Remember to convert to binary!')

%EOF
```